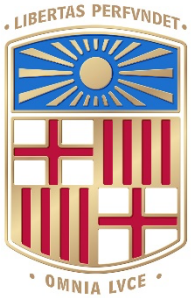

UNIVERSITAT DE BARCELONA

Final Degree Project

Biomedical Engineering Degree

"EEG-Based Functional Connectivity during Progression from Infantile Spasms to Lennox Gastaut Syndrome"

Barcelona, 06 de juny de 2022

Author: Blanca Romero Milà

Director/s: Dr. Beth Lopour

Tutor: Dr. Antonio Pardo Martínez

Abstract

Infantile Epileptic Spasms Syndrome (IESS) is a severe infantile epilepsy that can progress into Lennox-Gastaut Syndrome (LGS), associated with intellectual problems, and psychiatric disorders. Early diagnosis and treatment of LGS may improve prognosis [1]. There is a need for biomarkers to monitor the progression of these children. Based on prior work [2], [3], we hypothesize that functional connectivity strength is a robust biomarker for the presence of these epilepsies.

Five children diagnosed with IESS who progressed to LGS were included in this study. Functional connectivity networks were obtained by performing the statistical analysis of cross-correlation between electrode pairs [2]. The number of strong connections and the mean strength of the top 10% of connections were correlated to the disease state progression, response to treatment, and the child's age at the time of the EEG.

The number of strong connections and the mean connection strength gave approximately equivalent results. The connectivity strength was high at the time of IS and LGS diagnosis. Positive treatment outcome was associated with a decrease in strength, while an increase in strength reflected a worsening of the disease. Further, connectivity strength was not correlated to age, suggesting that these network changes are not due to age-related physiological changes.

Functional connectivity strength reflected the presence of IS and LGS, as well as positive or negative response to treatment. Computational EEG analysis of functional connectivity could be applied in clinical practice to improve the prognosis of LGS patients. However, it is critical to extend this analysis to a larger cohort of subjects to increase its power and validate these results.

Keywords:

Electroencephalography, epilepsy, infantile spasms, Lennox-Gastaut syndrome, functional connectivity, brain-mapping, resting-state network.

Acknowledgments

First, I would like to express my deepest gratitude to Dr. Lopour for giving me the opportunity of joining her research. From the moment I contacted her, she deposited her trust in me. Thank you for your advice, support, time, and patience. Special thanks also to all the members of the Lopouratory: Derek, Kavya, Trisha, Venus, and Chris. Thank you for making my stay so pleasant and for introducing me to the amazing world of epilepsy and computational neuroscience. Looking forward to working with you during the next years.

I would also like to express my sincere gratitude to Dr. Antonio Pardo Martínez, who has advised me through this process being beyond supportive of my project.

Further, I would like to thank Jordi Colomer for helping me with the logistics and structure of the thesis. I am thankful for his guidance and help.

Last but not least, on a more personal note, none of this would have been possible without the support of my family, friends, and partner. A special mention goes to Elena.

List of Figures

List of tables

TABLE OF CONTENTS

1. INTRODUCTION

1.1. PROJECT SCOPE

This research aims to evaluate the EEG-based functional connectivity of subjects during the progression from Infantile Epileptic Spasms Syndrome (IESS) to Lennox Gastaut Syndrome (LGS).

From previous knowledge (which will be presented in the following sections of the project), we hypothesize that the diagnosis of LGS will be directly related to an increase in functional connectivity, which will decrease after the resolution of epileptic encephalopathy with treatment.

This project has been carried out in the Laboratory of Computational and Translational Neuroscience of the Biomedical Engineering Department at the University of California Irvine, under the supervision of Dr. Lopour - associate professor at the Biomedical Engineering Department.

The main two limitations of this project are time and data availability. On one hand, the time span for the development of the project is six months, which limits the scope of the project. Further, the data used for this research project was provided by the Children's Hospital of Orange Country (CHOC). This data consists of ten patients which were diagnosed with IS and progressed to LGS. If we look at the demographic data of these pathologies, we can see that the incidence of ISs is around 0,035% for newborns [4], and this value decreases to 0,026% for LGS [5]. This explains the difficulty to gather data with the requirements needed for this research, which can difficult the process of drawing conclusions.

Finally, it is important to remark that this project does not aim to develop a commercial automatized system based on a microprocessor able to analyze EEG signals as a point of care device. This project will only focus on the processing and understanding of EEG data outside of the daily clinical context.

1.2. OBJECTIVES

The final objective of this research project is to:

Evaluate the EEG-based functional connectivity of subjects during the progression from Infantile Spasms (IS) to Lennox Gastaut Syndrome (LGS).

To achieve the final goal, it is essential to accomplish several intermediate goals which are:

- **Preprocessing of the EEG data**. Re-referencing, filtering, and artifact removal from EEG signals to increase the signal-to-noise ratio and ensure a correct interpretation of the data.
- **Computational analysis of the EEG data**. Calculation of the neuronal network and measurement of the functional connectivity of each EEG signal.

- **Determine the significance of the results**. Application of statistical testing to estimate the significance of the results obtained.
- **Answer the initial question and test the hypothesis.** Find a characteristic connectivity behavior potentially related to the progression from IS to LGS.

2. BACKGROUND

2.1. CLINICAL BACKGROUND

2.1.1. INFANTILE SPASMS SYNDROME

Infantile spasms (IS) refer to a type of epileptic encephalopathy that can be detected in children younger than 1-year-old. This syndrome is associated with epileptic spasms occurring in clusters whose most characteristic EEG finding is hypsarrhythmia. The spasms are usually associated with neurodegenerative symptoms such as developmental arrest or regression. The incidence of ISs is around 2-5/10.000 newborns; the prevalence is approximately 1-2/10.000 children at the age of 10 years; and the onset occurs at one year of life in 90% of cases with a male to female ratio of 6:4 [4].

Infantile spasms are characterized by brief muscle contractions, which involve the neck, the trunk, and the extremities in a symmetric bilateral manner. Individual spasms usually last between 1 and 5 seconds and are shown in clusters of 3-20 spasms which occur several times per day. Three different types of spasms can be differentiated using EEG video analysis: flexor, which results in jack-knifing at the waist and a self-hugging motion from adduction of the arms; extensor, an extension of the neck, trunk, and extremities; and mixed flexor-extensor, which involves a combination of neck, trunk, arm flexion and leg extension, or leg flexion and arm extension [6].

Infantile spasms are characterized by an interictal EEG pattern called hypsarrhythmia (Figure 1), which can be clearly differentiated from a normal EEG pattern in a healthy patient (Figure 3). Hypsarrhythmia was first defined by Gibbs and Gibbs [7] as asynchronous, non-rhythmic, and variable in duration and topography waves with a very high amplitude. The spikes consist of independent epileptiform discharges, which alternate between focal, multifocal, and generalized discharges at different points in time with a brief duration. Even though hypsarrhythmia assessment is the classic pattern used to diagnose this syndrome, it exhibits low interrater reliability for visually identifying the pattern and predicting future outcomes [8].

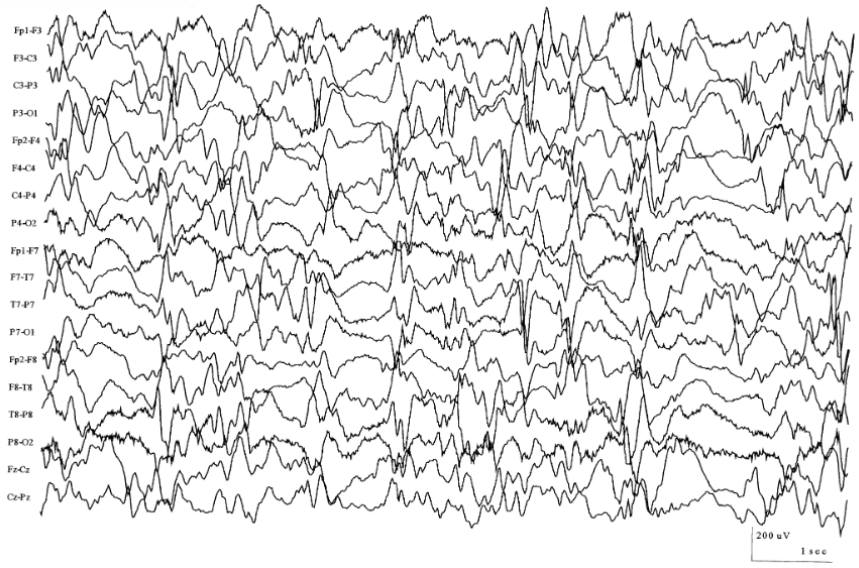

Figure 1: *Hypsarrhythmia in a 4-month-old female infant with cryptogenic infantile spams.* [6]

Due to the poor prognosis of infantile spasms, patients are usually treated aggressively after diagnosis, leading to serious side effects. There exists abundant literature about the treatment of infantile spasms. However, it is difficult for clinical trials to be reliable due to the ethical issues of performing placebo-controlled studies in kids and the uncontrolled clinical record of the disease. Some of the therapies that have been efficacious for infantile spasms are vigabatrin, adrenocorticotrophic hormone, prednisone, pyridoxine, or valproate [6].

Overall, patients with infantile spasms suffer from a poor outcome concerning chronic epilepsy, mental retardation, and other neurodevelopmental disabilities [6]. Around 70-90% of the patients suffer from mental retardation [9]. There is also a strong correlation between infantile spasms and Lennox-Gastaut syndrome (LGS). Some patients with infantile spasms in early infancy later develop LGS [10]. Approximately 20-50% of patients with infantile spasms evolve into LGS [11].

2.1.2. LENNOX GASTAUT SYNDROME

Lennox Gastaut Syndrome (LGS) is a severe childhood disorder characterized by encephalopathy and multiple seizure types [12]. LGS is defined by a triad of multiple drug-resistant seizure types, a specific electroencephalographic pattern with bursts of slow spike-wave (SSW) complexes or generalized paroxysmal fast activity (GPFA), and intellectual disability [13]. LGS prevalence is between 1 and 10% in patients with childhood epilepsies. For the diagnosis of LGS, the criteria are that the patient had onset of multiple seizure types before 11-year-old, with at least one seizure type resulting in falls, and an EEG with SSW complexes. LGS prevalence is estimated to be 0.26/1000 at 10 years old. Finally, 91% of patients with LGS suffer from intellectual disabilities [13], [14]. Furthermore, 80-90% of onsets are around 8 years of life, and the male to female ratio is around 1.55 [5], [15].

LGS patients are characterized for having profound deleterious effects on intellectual and psychosocial functions. About 20-60% of the patients show cognitive impairments at the time of diagnosis, which becomes more apparent over time. After 5 years of onset, 75-90% of patients have severe intellectual problems. Furthermore, many patients develop behavioral and psychiatric disorders such as attentional problems, aggression, and autistic features. Regarding seizures, the most abundant types in LGS are tonic and atypical absence seizures [16]. The second most abundant seizure type is atypical absences; epileptic drop attacks are particularly hazardous and occur in more than half of the patients, which could be the result of tonic, atonic, or even myoclonic seizures; about two-thirds of patients have episodes of nonconvulsive status epilepticus, prolonged atypical absences with varying degrees of altered consciousness periodically interrupted by brief tonic seizures [13].

Lennox Gastaut is characterized by slow (<2.5 Hz) spike-and-wave (SSW) complexes with an abnormally slow background activity (Figure 2). The spikes are usually broad and around 70-200 milliseconds [16]. Not every slow wave is preceded by a spike or sharp wave, and the bursts of SSW complexes may be remarkably irregular without an apparent onset and offset. During sleep, diffuse or bilateral fast (10-25 Hz) rhythm patterns can be recorded, which are called generalized paroxysmal fast activity (GPFA) (Figure 2). They last for a few seconds and are composed of brief identical and shorter intervals [13].

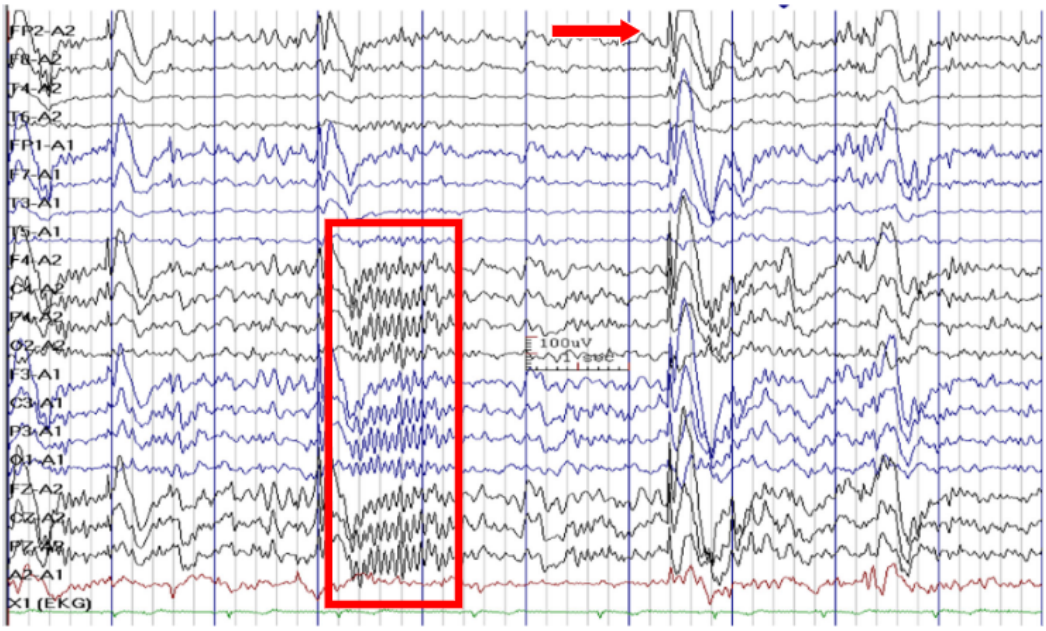

Figure 2: *Slow spike-waves (arrow) and generalized paroxysmal fast activity (box) in Lennox-Gastaut syndrome.* [13]

Usually, LGS patients suffer from seizures resistant to antiepileptic drugs. Therefore, the primary objective is to reduce in frequency the most incapacitating and injurious seizures like drop attacks and tonic-clonic seizures. Valproate is the first treatment of choice in patients with LGS, followed by topiramate, lamotrigine, or clobazam. There are other alternative agents such as cannabidiol, steroids, or intravenous immunoglobulin. Furthermore, the ketogenic diet is effective in children with LGS. It consists of a high-fat, low-protein, and low-carbohydrate diet which is thought to alter the fundamental biochemistry of neurons, reducing neuronal excitability. As previously mentioned, LGS is drug-resistant for most patients, which results in a poor prognosis despite the ongoing investigation into drug treatments. Therefore, brain surgery is the only option to control seizures, where seizure foci are removed successfully. This procedure is only possible when the epileptiform discharges come from the same brain area and are removable. However, resective brain surgery is rarely an option in patients with LGS, who often have a diffuse or multifocal brain abnormality [13].

For LGS patients, the long-term outcome is generally poor, and complete seizure freedom is usually not achieved. LGS is generally associated with long-term adverse effects on intellectual development, social functioning, and independent living, impacting facility members and caregivers. Timely diagnosis and appropriate treatments might result in improved outcomes and less costly management in patients affected with LGS.

2.1.3. EEG SIGNAL

2.1.3.1. EEG SIGNAL CHARACTERISTICS

To study the encephalopathies described above, clinicians usually use the electroencephalography (EEG) signal. Therefore, it is essential to understand its meaning and the correlations with the behavior of the brain.

The human brain has about 100 billion neurons, each of which has about 10,000 connections with other neurons. This active neuronal network can be divided into many subnetworks with ionic currents, which cause local extracellular potential changes. The superposition of these differences in potentials is named local field potential (LFP). The primary sources of LFP are synaptic transmissions and action potentials (APs), having a broad frequency spectrum up to several hundred Hertz. Synaptic transmissions are the source of low-frequency components, and APs the source of high-frequency components. If ohmic impedances and electric dipole sources are assumed, the contribution of a single source to the LFP decays with the square of the distance. Therefore, nearby sources contribute most, and contributions from distant sources are subject to strong attenuation.

The electroencephalogram (EEG) (Figure 3) is the most common noninvasive method for recording brain activity, which measures the brain potentials using different types of electrodes located on the scalp of the patients. The signal recorded using scalp electrodes is a modified version of LFPs for two main reasons. First, as previously mentioned, since the electric field decays with the square of the distance from the source, the LFP is significantly attenuated when it reaches the scalp. In the second place, the volume conductance of the different tissues (brain, cerebral fluid, skull, and scalp) causes spatial smoothing of the signal. Due to this, scalp recording will only acquire signals from synchronous brain activity. The larger the synchronously active cell population, the higher the amplitude in the EEG. Therefore, it is crucial to consider that EEG oscillations recorded at the scalp only represent a subset of the electrical brain activity at a particular point in time [17].

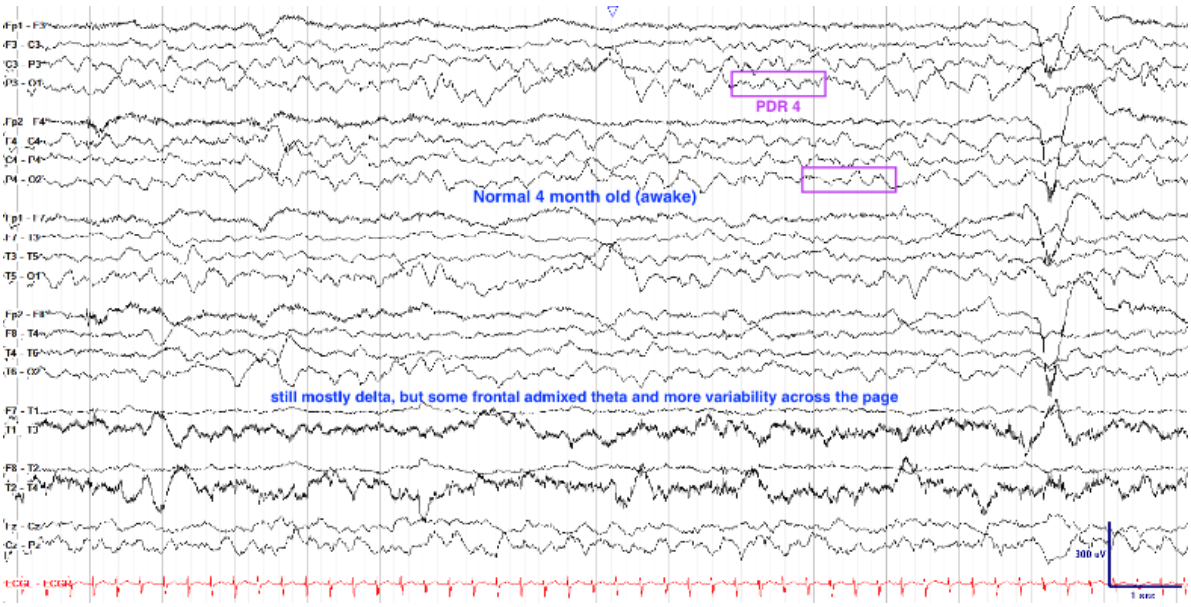

Figure 3: Normal EEG for an awake 4 month old subject [18].

2.1.3.2. SPONTANEOUS EEG

The spontaneous EEG is the measurable part of brain activity that goes on permanently in the living individual. In a healthy waking brain, the peak-to-peak amplitude of the signal is under 75μV. Furthermore, an important portion of the signal power comes from rhythmic oscillations in a frequency

bandwidth from 1Hz to 40Hz. This wide frequency range is divided into different functional ranges associated to names [17] (Figure 4).

- **Gamma oscillations** (30-100Hz): Associated with arousal and perceptual binding mechanisms. For instance, integration of various aspects of a stimulus into a coherent overall perception.
- **Beta oscillations** (13-30 Hz): Related to different mental states like active concentration, task engagement, excitement, anxiety, attention, or vigilance, as well as sensorimotor activity. The amplitude is usually in the μV.
- **Alpha oscillations** (8-13 Hz): Indicate state of relaxed wakefulness, they are also common during resting periods in which people have their eyes closed. The amplitude of these oscillations is typically large, up to several tens of μV.
- **Theta oscillations** (4-8 Hz): associated with specific sleep states, or meditation. Also, it can be related to directed attention towards a specific stimulus.
- **Delta oscillations** (below 1-4 Hz): deep and unconscious sleep in healthy humans.

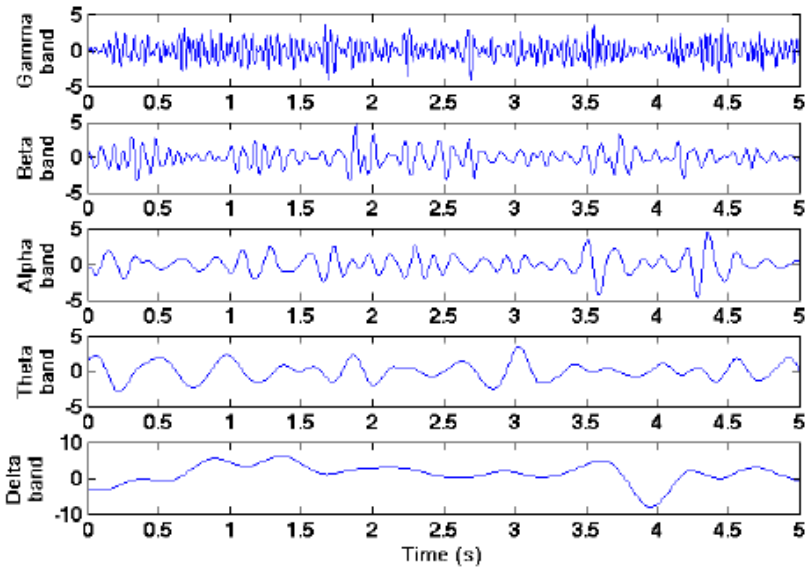

Figure 4: The five frequency bands of an EEG signal: gamma, beta, alpha, theta, and delta. [19]

2.2. STATE OF THE ART

2.2.1. COMPUTATIONAL ANALYSIS ON INFANTILE SPASMS

To date, the diagnosis of infantile spasms (IS) is based on evaluating clinical events correlated to ictal EEG hypsarrhythmia pattern and spike quantification. A correct and early diagnosis of IS enables the prescription of first-line treatments, which is associated with a better prognosis of the disease [20]. Therefore, it is essential to rely on techniques that ensure a quantifiable and reliable IS diagnosis.

It has been shown that the hypsarrhythmia pattern may not be a reliable marker for diagnosis since it is not always present in IS patients and it has a low inter rater reliability (IRR) [8]. Two new approaches have been presented for IS diagnosis based on visual inspection (Appendix 1, Table 1). First, paroxysmal fast activity (PFAs) – events in the beta and gamma frequency bands that last between 200ms and 8s and occur around 1 to >100 times in a 20min interictal non-REM sleep period - has been shown to indicate high risk for epilepsy when detected in EEG signals, but they are not always present and they are not IS specific [21]. Secondly, BASED score – an interictal EEG grading scale to identify children with IS - has shown to have a higher IRR than any other hypsarrhythmia quantification method [22], [23]. On the other hand, several quantitative methods (Appendix 1, Table 2) like functional connectivity [2], [3], [24]–[30], power spectrum [2], [28], [31] or HFOs [32]–[38] have been developed to assess IS diagnosis. Most of these tools have shown to correlate with clinicians-diagnostic assessments, but further studies are needed to solve some existing inconsistencies.

Clinically, treatment outcome of IS is assessed based on the cessation of clinical spasms and resolution of hypsarrhythmia [39]. Treatment outcome assessment describes the changes in a patient's condition after treatments. Therefore, determining the effects of a therapy on a patient is essential to realign the treatment path when necessary. Further, it has been seen that using hypsarrhythmia to assess it has a low IRR [20]. Therefore, the BASED score has been presented as an alternative for the evaluation of responders with a higher IR [23]. Further, computational techniques (Appendix 1, Table 2)) like functional connectivity [40], power spectrum [41], and HFOs [35]–[37], [42] have been testes as potential markers of treatment outcome, showing differentiative traits between responders and non/responders but with still some inconsistencies. Therefore, further studies are needed to develop more reliable and objective measures.

Finally, treatment prediction allows clinicians to make decisions about therapy objectively, accounting for the variability between IS patients. Further, long-term prognosis and relapse assessment would enable a faster treatment change in the patients who require it. The hypsarrhythmia EEG pattern has shown not to be a tool to predict treatment outcome, and no alternative visual inspection methods have been presented. On the other hand, the BASED score has been proposed as a tool for assessing long-term prognosis and relapse [43], as well as identifying epileptic discharges in the EEG signal[44], [45]. Also, very few computational analysis methods (Appendix 1, Table 2)) have been developed for treatment prediction, long-term outcome, and relapse. Functional connectivity [40], power spectrum [41], HFOs [37], [42], [46] and entropy [47], within others, have shown to be potential markers for treatment prediction.

2.2.2. STUDIES ABOUT THE TRANSITION FROM IS TO LGS

There exist very few studies that analyze the evolution of Infantile Spasms (or West Syndrome) to Lennox-Gastaut Syndrome. In these studies, they report that 30-60% of IS patients evolve to LGS [48]–[51].

In 2009, a study published by You et al. reported that ketogenic diet, prednisolone or adrenocorticotropic hormone treatments could be related with a decrease in the evolution of IS to LGS [50]. Further, in 2018 a study stated that vigabatrin could also be related to a lower rate of LGS in IS

patients [51]. However, a study published in 2021 has declined the two hypothesis mentioned above stating that no significant difference was found between patients under different treatments. However, this study found some significant results. They state that some risk factors for the development of LGS are developmental delay and seizures prior to the onset of IS, as well as a poor response to the first IS treatment. Further, no significant results were obtained concerning different IS treatments, response to subsequent treatments for IS, or etiology [48].

Additionally, the electroclinical pattern of patients transitioning from IS to LGS has been divided into four well-defined groups: the first group refers to subjects with multiple seizure types, including epileptic spasms associated with multifocal paroxysm; the second group includes patients with mainly focal seizures associated with focal discharges; the third group describes subjects with predominance of epileptic spasms and myoclonic seizures associated with diffuse spike-and=wave and polyspike-and-wave paroxysms; finally, group four englobes electroclinical patterns that are a mix of the three previous groups [49].

As it can be seen, the studies mentioned above study the evolution from IS to LGS in a subjective manner. They try to correlate etiology, therapies or treatment outcome with the evolution from one disease to the other. However, there are no studies computationally analyzing this evolution, or obtaining a quantifiable marker to predict or assess the onset of LGS in IS patients. As it has been stated in this project, LGS is a severe encephalopathy, and patients rarely achieve a seizure-free outcome. Therefore, an early diagnosis of LGS or a prediction of this IS-LGS evolution would imply an earlier prescription of treatment, which has been shown to be related with a better long-term outcome and prognosis.

3. CONCEPT ENGINEERING

3.1. DATA ACQUISITION TECHNIQUES

The data coming from the brain can be acquired using different techniques, which differ in resolution, invasiveness, and precision, within others. Some of these tools are presented as follows.

3.1.1. ELECTROENCEPHALOGRAPHY (EEG)

Electroencephalography (EEG) is a non-invasive technique that provides direct real-time information about the electrical activity of the brain. EEG uses scalp electrodes to record brain signals. The amplitude of these signals is between 5-300 μV, with a frequency lower than 100 Hz. EEG signals have a low spatial resolution and a medium temporal resolution, compared to other techniques [52]. One of the main downfalls of this technique is that it is not able to capture signals from deep structures of the brain, and it suffers from the volume conduction effect [53].

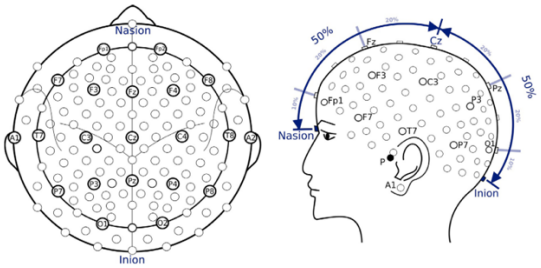

Figure 5 Scheme of the location of the electrodes on the scalp with a 10-5 electrode system [52].

3.1.2. INTRACRANIAL ELECTROENCEPHALOGRAPHY (iEEG)

Intracranial EEG (iEEG) – which is also known as electrocorticography (ECoG) when using subdural grid electrodes or stereotactic EEG (sEEG) when using depth electrodes – is an invasive direct measurement of brain electrical activity with electrodes located in the brain tissue. It provides anatomically precise (high spatial resolution) information of neuron activity with a relatively high temporal scale. This technique requires a surgical procedure to locate the electrodes in the target region [54].

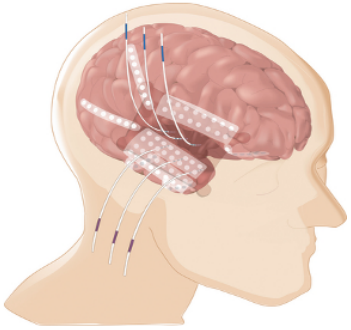

Figure 6 Schematic drawing of the implantation of subdural and depth electrodes [55].

3.1.3 MAGNETOENCEPHALOGRAPHY (MEG)

Magnetoencephalography (MEG) is a non-invasive test that measures the magnetic field generated by the electrical activity of the neurons. The fields that are being measured are in the range of femto- to pico-tesla. Referring to resolution, MEG offers a very high temporal resolution and good spatial resolution. The MEG recording machine has high dimensions and the infrastructures needed to use a MEG are very complex - to attenuate the magnetic noise of the environment it is located inside of a shielded room [56].

Figure 7 Magnetoencephalogram machine [56].

3.1.4 FUNCTIONAL MAGNETIC RESONANCE IMAGING (FMRI)

Functional Magnetic Resonance Imaging (fMRI) is a non-invasive technique that indirectly measures the brain activity. Specifically, the Blood Oxygen Level Development (BOLD) technique studies the changes in deoxyhemoglobin concentration, which depends on the metabolism of neurons and therefore it is related to its electrical activity. This technique allows to obtain a good spatial resolution but has a low temporal resolution – which can be desired in some experiments. The fMRI machine has large dimensions and requires a complex infrastructure and isolation from external magnetic fields [57].

Figure 8 Magnetic Resonance Machine [58].

3.1.4 TECHNIQUES' COMPARISON

The table fellow summarizes the relevant features of the four recording techniques explained above. The characteristics studied will be decisive to further chose the technique that better suits this project.

	EEG	iEEG	MEG	fMRI
Invasive	No	Yes	No	No
Temporal resolution	Medium	Medium	High	Low
Spatial resolution	Low	Medium	Low	Medium
Cost	Low	High	High	High
Accessibility	High	Low	Low	Medium

Table 1 Recording techniques comparative table.

Now, we are going to analyze each of the features to choose the best fitting technique. First, it is relevant to consider that we are studying a very specific and rare disease. Therefore, the number of patients available are limited. For this, it is important that the recording technique is accessible and non-invasive, so that we can acquire as much data as possible. If we look at the non-technical features – invasiveness, cost, and accessibility- we can note that the EEG is the one that better suits is requirements. However, the electroencephalogram has a relatively low temporal and spatial resolution. These characteristics will not affect our study for the two following reasons:

- **Temporal resolution:** we want to study resting EEG. Therefore, the subjects will not be doing any activities, or processing any stimuli, which decreases the importance of a high temporal resolution.
- **Spatial resolution:** we want to characterize the overall functional connectivity of the brain, how different regions of the brain are connected to each other. Therefore, a high spatial resolution is not needed either.

3.2. EEG FILTERING

EEG signals are recorded using amplifiers, which measure the electrical activity at one electrode relative to another, eliminating a significant amount of the common activity between the electrodes. If we think of artifacts, biological and technical, they are usually similar around the head. Therefore, it will often be eliminated using differential amplifiers. This method reduces the noise, increasing the signal-to-noise ratio in the recording. Also, the amplifier increases the voltage difference of the signal to increase the detection range and improve detection. Finally, the EEG recording machine converts the analog signal is converted into a digital signal so we can further work with it.

Further, filters are used to select the information of interest. For this, filters usually allow to keep the frequency bands of interest. We can define four ways of using filters to highlight frequencies of interest: bandpass, band-stop, high-pass, and low-pass. Bandpass filters allow to keep activity between two specified frequencies, while band-stop filters remove the activity between two frequency

values. On the other hand, high-pass and low pass retain active above or below a frequency value, respectively.

Overall, the filters used for EEG signals can be classified in two groups: finite impulse response (FIR) filters and infinite impulse response (IIR) filters [59].

3.2.1. FINITE IMPULSE RESPONSE (FIR) FILTERS

Finite impulse response (FIR) filters offer a response to an impulse that will be a finite response in time. Equation 1 shows the structure of an FIR filter, a finite summation of the input signal with a finite delay in time (x (n-k)) weighted with specific coefficients (b).

$$y(n) = \sum_{k=1}^{N} b_k x(n-k) \qquad \text{Eq. 1}$$

Therefore, the output of an FIR filter is a simple weighted average of a certain number of past input samples only. In opposition to the infinite response filters (IIR)FIR filters do not implement feedback loops. Regardless of the type of signal input to the filter or for how long we apply a signal to the filter, FIR filters never become unstable [59].

3.2.2. INFINITE IMPULSE RESPONSE (IIR) FILTERS

Infinite impulse response (IIR) filters include a feedback component to the FIR structure. They are considered recursive filters since, in addition to current and previous input values, they also use previous output values to generate the result. IIR filters use many numbers of previous outputs, generating an infinite response to an impulse.

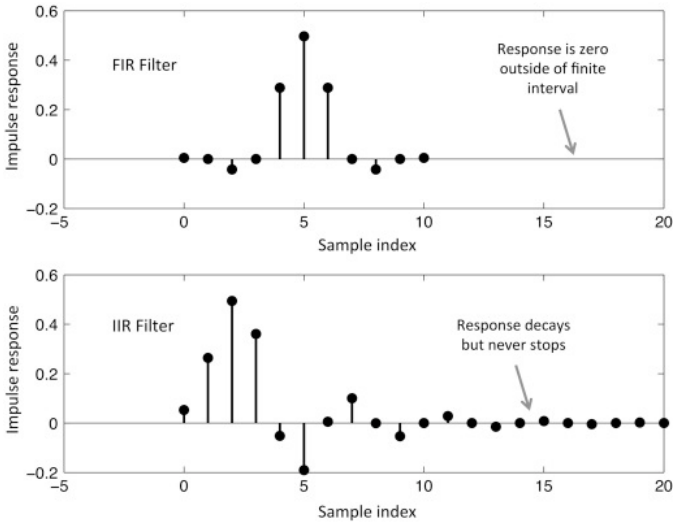

Figure 9 Impulse response of a Finite Impulse Response (FIR) filter vs. an Infinite Impulse Response (IIR) filter [60].

Mathematically, they can be written equivalently to FIR filters, but the summation over time is infinite (equation 2). Furthermore, this dependence on previous outputs avoids IIR filters from having a linear phase. The main difference between an FIR and an IIR filter is that FIR can be designed with a linear phase, while IIRs cannot. Therefore, IIRs will suffer from a phase distortion which can affect the data. Additionally, in the IIR filter design, attention must be paid to the value of the coefficients to prevent instabilities, otherwise, the output will cause oscillations that increase exponentially [59].

$$\sum_{m=0}^{M} a_m y(n-m) = \sum_{k=0}^{N} b_k x(n-k) \qquad \text{Eq. 2}$$

3.3. EEG ARTIFACT DETECTION

When working with EEG, it is essential to preprocess the data to obtain a clean signal. Despite this, there can always be some artifacts remaining that need to be considered. Artifacts can be divided into two groups: biological and technical.

Physiological artifacts mainly consist of muscle – electromyogram (EMG) – activities (e.g., neck, face), eye blinks, and eye movements (Figure 10) – electrooculogram (EOG). Furthermore, sweating can produce a drift of the zero line of the signal. EMG occurs between 20 and 1500 Hz, while EOG covers the low frequencies from DC to 10Hz. Artifacts must be detected and indicated in an online system, and they can then be marked or removed.

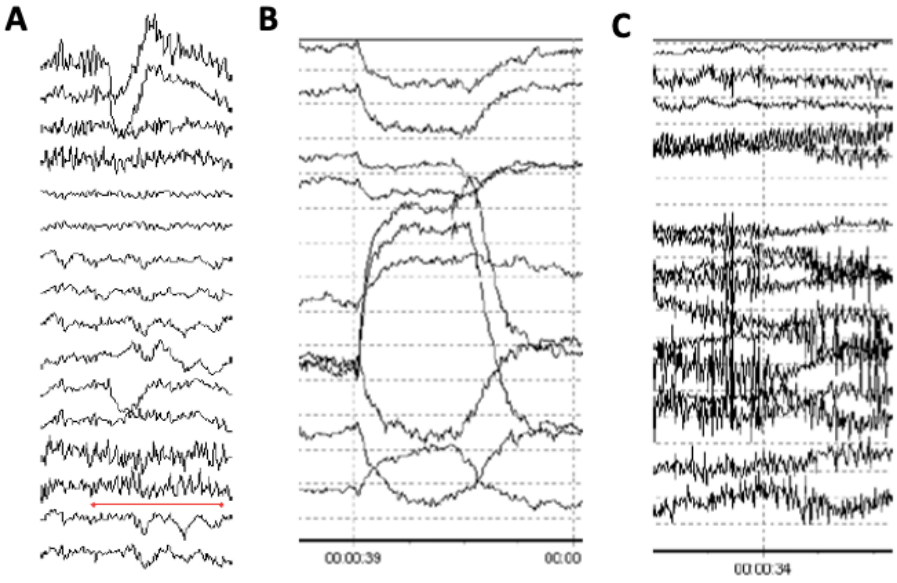

Figure 10 Examples of physiological artifacts. (A) Eye blink. (B) Eye movement. (C) Muscle artifacts.

On the other hand, technical artifacts (Figure 11) are external electrical and electromagnetic noise coming from power lines, electric lights, or other fields. Furthermore, poor contact between the electrodes and the patients' skin produces high impedances, increasing the artifacts. Finally, when

choosing the electrodes, if the material used is not adequate, it can act as a high pass filter, hiding the signals of interest. To overcome technical artifacts, several techniques like shielding the recording system, using filters (e.g., notch filters to remove the power line noise), and high-quality amplifiers [17].

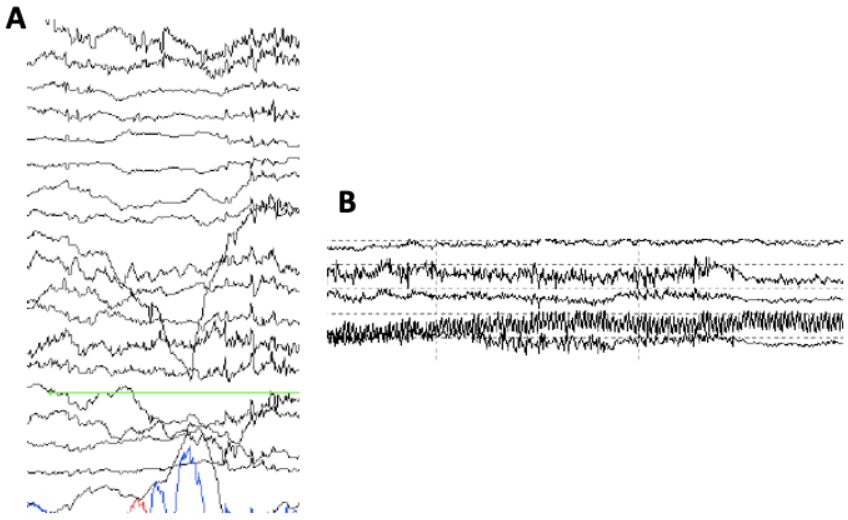

Figure 11 Examples of technical artifacts. (A) Electrode movement. (B) Power line artifact.

3.3.1. VISUAL INSPECTION

One way of detecting fragments of data with artifacts is by visual inspection. In this scenario, board-certified pediatric epileptologists (DS) review the EEG data and mark artifacts manually. These artifacts can be due to eye blinks, movement, poor electrode contact, or muscle activity. Afterwards, segments of data with artifacts are usually removed [40], [61]–[63].

3.3.2. AUTOMATED ARTIFACT DETECTION

Marking artifacts manually is a very time-consuming task, and it is tied to a high level of subjection, increasing variability within different professionals and studies. For this, there have been developed some tools so automatically detect these artifacts by using objective mathematical calculations.

In 2003, Durka et al. [64] presented a tool to detect EEG artifacts in polysomnographic recordings. For this artifact detector, they selected different types of artifacts for which a relevant parameter was calculated for a given epoch. From here, if any of the parameters exceeded a predefined threshold, the epoch was marked as an artifact. Three examples of artifacts considered, and their parameters are the following:

- **Eyeblinks**: Correlations between bipolar derivations Fp1-F3 and F3-C3 (left hemisphere) and between Fp2-F4 and F4-C4 (right hemisphere) were computed in 1.5 seconds epochs, with overlapping windows moved by 1 second. The largest of these correlations was taken as parameter representing eyeblinks. If any of the correlations exceeded the threshold (default 0.875), the window was marked as artifact.

- **Power Supply**: Spectral power from 48 to 52 Hz (Europe), calculated in 1-second epochs, was divided by the total power of the corresponding epoch. If this value exceeded a threshold of 0.325 (default value), the 4 seconds epoch was marked as an artifact.

- **Muscle activity**: For each EEG channel, spectral power from 40 Hz to the Nyquist frequency was normalized to the total power with the exclusion of the power around 50 Hz (ac frequency in Europe). The allowed range for the threshold is ($m_{0.5}$ + 1.5σ, $m_{0.5}$ + 6 σ) with default in the middle of this range. $m_{0.5}$ and σ denote median and variance estimated separately for each channel. If the value of this parameter exceeded the threshold for any 1-second epoch, all the 4 seconds window was an artifact.

There exist other automatic artifact detectors, like the software package presented by Kramer et al. in 2003. This software selects EEG data from EOG, EMG, and EEG artifacts in event-related potentials [65].

3.4. NETWORK CONSTRUCTION: EEG-BASED FUNCTIONAL CONNECTIVITY

A network can be defined as a collection of nodes and edges. A node represents a participant or actor in the network, while an edge represents a link or association between two nodes. In a neural network, the node represents individual neurons or regions of the brain, and the edges consist of the connections between neurons or brain regions. The linking between two nodes can be determined by a physical connection or can represent less obvious connections. In some cases, the interaction between nodes may only be observed through dynamic activity at individual nodes, which need to be calculated by applying coupling measures to multivariate time series data, aiming to infer these associations.

From a statistical perspective, the two main difficulties of this kind of studies is to correctly interpret the coupling results in declaring network edges and, also, the accurate quantification of the uncertainty associated with the resulting networks. One of the simplest ways of studying coupling consists of comparing coupling strengths to a threshold value. When the coupling strength between two nodes exceeds a predefined threshold, the two nodes are then connected with an edge. The figure below (Figure 12) clearly represents the different results that can be obtained from the same data depending on the threshold value [66].

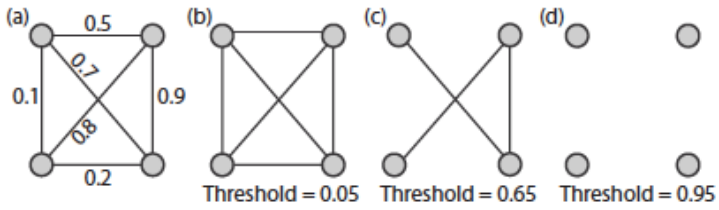

Figure 12 Each grey circle represents a node (a spatial location), and each line represents an edge. Each figure represents the number of connections (edges) over the corresponding threshold [66].

There exist different coupling measures based on diverse concepts. Different options will be presented as follows.

3.4.1. PHASE LAG INDEX (PLI)

Phase Lag Index (PLI) is a measure of phase synchronization exploiting the asymmetry of the distribution of instantaneous phase differences between two signals [67]. Therefore, PLI (Eq. 3) is used to measure synchronization between the recording electrodes.

$$\mathrm{PLI} = \left| \frac{1}{N} \sum_{n=1}^{N} sign(\Delta\varphi(t_n)) \right| \qquad \text{Eq. 3}$$

The Hilbert transform of the filtered EEG is computed foreach channel and epoch to calculate the instantaneous phase in the alpha band. For each channel pair in a time window, PLI calculates the mean signum of the instantaneous phase difference between the two channels at time n, which is denoted $\Delta\varphi(t_n)$. The PLI values go from zero - symmetrical phase difference between the two signals -, to one – asymmetrical phase difference between the two signals.

When calculating the PLI for each channel, we obtain a N-by-N adjacency matrix, where N is the number of electrodes, where each element represents the phase synchronization between the respective channel pair. Then, the adjacency matrices over all epochs are averaged to calculate the functional connectivity of a subject.

At the same time, surrogate data analysis is performed to determine the significant connection pairs in the mean adjacency matrix. To generate the surrogate data, the Fourier transform is performed for each electrode in each epoch, and the data was permuted in the frequency domain to shuffle the phases while retaining the original amplitude profile of the EEG signal. Then, the signal is converted back to the time domain by using the inverse Fourier transform, and the PLI is calculated using this new signal. All this process is done 100 times creating a null distribution of PLI values for each electrode pair, in which the pairs have no phase-based relationship.

Finally, the mean adjacency matrix is compared to the 95th percentile of the surrogate data, discarding any insignificant connections [68].

The following figure (Figure 13) summarizes the procedure explained above for the calculation of functional connectivity using PLI for a 31-electrodes recording.

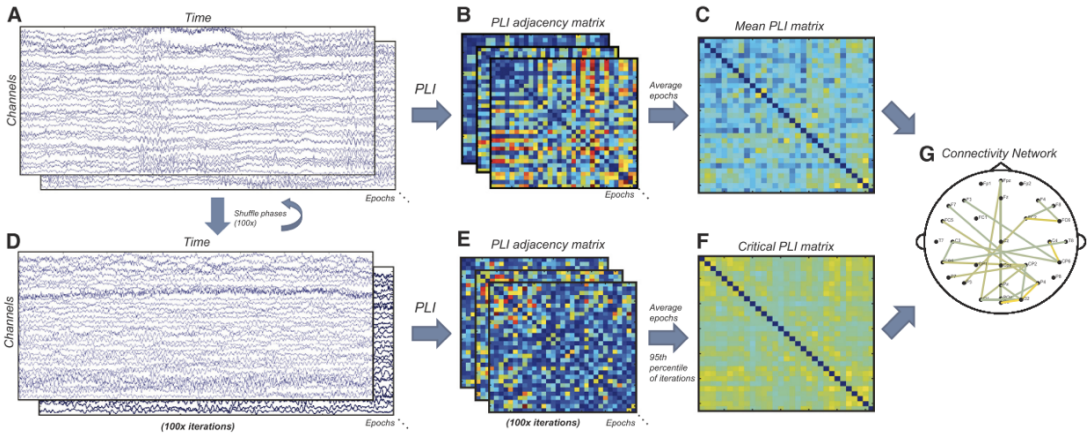

Figure 13 Summary figure of the functional connectivity calculations with PLI. (A) Raw EEG data is separated into time epochs. (B) PLI results for each epoch. (C) Mean of the PLI matrices. (D) 100 iterations of shuffled data for significance calculations, (E) PLI calculation, and (F) average. (G) The critical values are compared to the original mean PLI matrix to obtain final connections [68].

3.4.2. CROSS CORRELATION

Cross correlation consists of a linear coupling measure in which, for a pair of time series $x_i[t]$ and $x_j[t]$ of lengths n, the sample cross correlation at lag τ is defined as (Eq. 4):

$$C_{ij}[\tau] = \frac{1}{\sigma_i \sigma_j (n - 2\tau)} \sum_{t=1}^{n-\tau} (x_i[t] - \bar{x_i})(x_j[t + \tau] - \bar{x_j}) \qquad \text{Eq. 4}$$

Where $\bar{x}_i$ and $\bar{x}_j$ are the averages and $\hat{\sigma}_i$, and $\hat{\sigma}_j$ are the standard deviations of $x_i[t]$ and $x_j[t]$, respectively, estimated from the data. More precisely, what needs to be computed is the maximal cross correlation (Eq. 5), the maximum of the absolute value of Cij[τ] over τ. This measure serves as the statistic for testing whether to assign an edge between nodes i and j, for each pair of nodes.

$$s_{ij} = max_\tau \left| C_{ij}[\tau] \right| \qquad \text{Eq. 5}$$

After obtaining the value of the maximum cross correlation for each pair of nodes, it is crucial to perform a significance test to decide if the network edge is included. We use s_{ij} to test the null hypothesis that $x_i[t]$ and $x_j[t]$ are uncorrelated against the alternative hypothesis that they are correlated. Then, the p-value can be computed using two different methods: an analytic method and a frequency domain bootstrap method [66].

Referring to EEG functional connectivity, we aim to identify the maximum cross correlation within each one second window of data, with a certain maximum time lag. After the cross correlation calculation, we define the connection strength for each electrode pair of the data. The strength is defined as the fraction of one second epochs that were significant, ranging from zero (never significant) to one (always significant) [40]. This information can be represented in cross correlation matrices or using a connectivity plot (Figure 14).

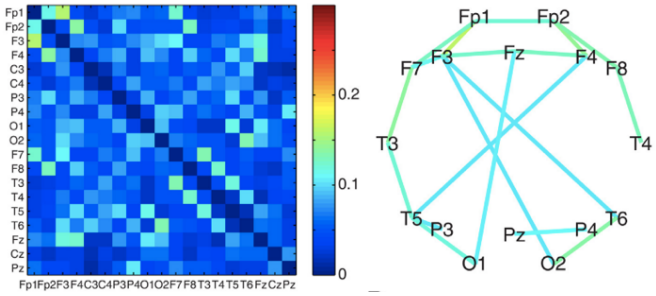

Figure 14 Cross-correlation heat map (left) and connectivity plot (right) [40].

3.4.3. MINIMUM SPANNING TREE (MST)

Minimum Spanning Tree (MST) consists of a unique acyclic subnetwork that contains most of the strongest connections of an original, weighted network. For instance, we first calculate the PLI of the EEG data. Then, Kruskal's algorithm is used to compute the MST, which orders the weights of all edges, starting the construction of an MST from there. A series of events are performed as many times as possible: adding the edge with the highest PLI until all nodes N are connected in a loopless network consisting of N-1 edges. It is important to consider that if adding one edge results in the formation of a cycle within the network, this edge will not be considered. The figure below (Figure 15) represents the connectivity network generated using the PLI method (middle) and the correspondent MST network (right). The MST keeps the connections with higher strength and ensure that all nodes have a maximum of two edges and that the overall connectivity is not cyclic.

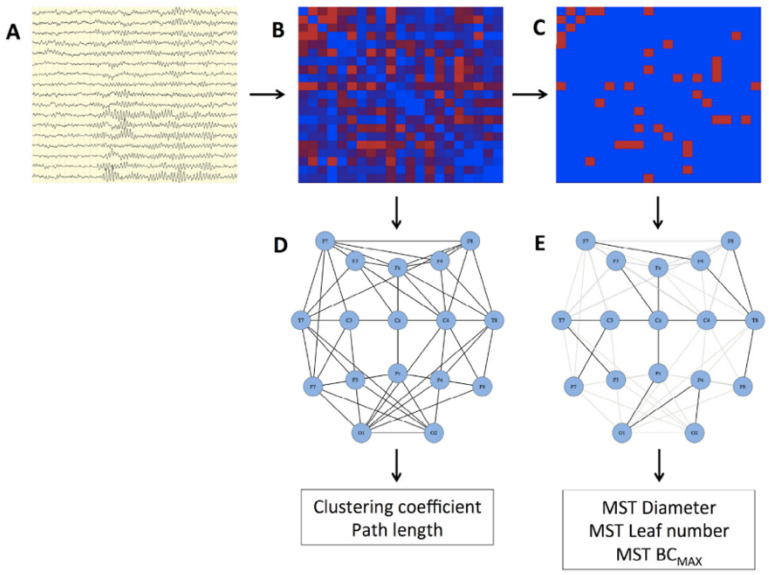

Figure 15 Schematics of the creation of a functional network. (A) Raw EEG data. (B) Mean PLI matrix and (D) connectivity plot from PLI matrix. (C) Minimum spanning tree derived from the PLI matrix and (E) minimum spanning tree connectivity plot (dark lines) [26].

Further, two parameters are calculated. First, the leaf number consists of the number of nodes in the tree with degree = 1 – electrodes connected by only one edge to the network. The leaf number refers to an upper bound to the diameter of the spanning tree that is the largest distance between any

possible pair of nodes of the tree. On the other hand, we also define the upper limit of the diameter. The largest possible diameter will decrease with increasing leaf number [26].

3.5. SOFTWARE

To undergo the preprocessing methods and connectivity calculation explained above, different software can be used. The most common options are the ones presented as follows.

3.5.1. R

The R software is an open-source environment designed for statistical computing and graphics. It is usually used by data miners and statisticians to undergo data analysis and develop complex statistical algorithms in fields ranging from computational biology to political science. The exist several R packages that contain numerous functions in the R language [69].

3.5.2. MATLAB

MATLAB is a programming language and numeric computing environment which allows a wide range of processes such as manipulation of matrices, plotting of functions and data, implementation of algorithms or creation of user interfaces. The main objective of MATLAB is numeric computing, but it has additional tools that allow symbolic computing abilities and simulation of model-based designs. This software is used in many fields like engineering, science, and economics [70].

3.5.3. PYTHON

Python is a general purpose and Object-Oriented programming language that has a design aimed for an improvement of code readability, obtaining a clear and logical code. Python has built-in high level data types such as strings, lists or dictionaries. It also has multiple levels of organization with functions, classes, modules, and packages [71].

3.6. WORKFLOW AND SOLUTION PRIORITIZATION

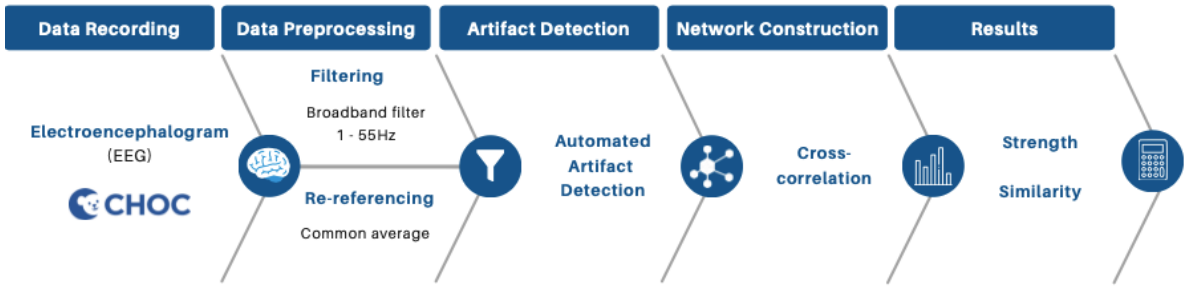

Figure 16 Workflow diagram: data recording, data preprocessing, artifact detection, network construction, and results.

The scheme above (Figure 16) represents the workflow needed for the development of the project. All the processes will be done using MATLAB software. This is the standard software used in the Laboratory of Computational and Translational Neuroscience at UCI, and all the existing code is already in this language. Therefore, switching the software would imply increasing the difficulties of the project without a specific purpose. Further, MATLAB already has several built-in functions and packages for signal processing.

Secondly, as exposed in 3.1.4., the signals used will consist of electroencephalograms (EEGs). Afterward, a broadband filter will be applied, with automated artifact detection. Then, the network will be constructed using cross-correlation, determining its significance. Finally, to show the results, the strength of the connections will be computed, also, the similarity of the different functional networks will be analyzed. The reasoning behind the selection of this preprocessing tools will be discussed in section 4.2.

Data acquisition	Filtering	Artifact detection	Network construction
1. EEG 2. iEEG *MEG *fMRI	1. Broadband	1. Automated 2. Visual Inspection	1. Cross-correlation 2. Phase Lag Index 3. Minimum Spanning Tree

Table 2 Solution prioritization. The first option is to acquire EEG data, broadband filter it, remove the artifacts automatically, and calculate the connectivity network using cross-correlation.

Referring to solution prioritization, we can arrange the tools described in concept engineering (Table 2). For data acquisition, the data used will be EEG. In case this data was not available, we could also use iEEG signals, but it is an invasive method and more difficult to obtain. Further, MEG and fMRI data are not considered for this project. With respect to the filter, we are going to apply a broadband filter from 1 to 55 Hz, which is the frequency range we are interested in when wanting to calculate functional networks. Further, the filter will be a finite impulse response (FIR) filter, since they are more stable (they also require more computational power, but this is not an impediment for nowadays computers). To detect artifacts, an automated detector will be used. In case the detector doesn't work properly, artifacts could be selected by visual inspection. Finally, for constructing the network, cross-correlation is the first option to apply. In case we don't obtain significant results using this tool, PLI and MST could be applied.

4. DETAIL ENGINEERING

With respect to the programming language, the project will be developed using MATLAB, which is the language of preference of the Laboratory of Computational and Translational Neuroscience of the University of California Irvine. All the code already existing has been developed using MATLAB language. Therefore, switching the programming language would considerably increase the difficulty of the project. Further, the MATLAB software toolchain includes various built-in functions and packages for signal processing.

4.1. EEG ACQUISITION

EEG data collection is done through scalp EEG electrodes using the International 10-20 system of electrode placement (Figure 17). This technique is non-invasive, decreasing the risks to which the patients are exposed. Further, all epilepsy patients undergo one or several EEGs during their follow-up, increasing the availability of this type of data.

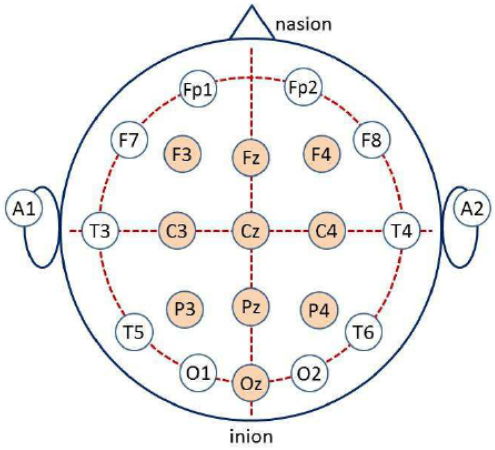

Figure 17 International 10-20 system of electrode placement.

The data used consists of awake data and the recording minimum time is around 15 minutes.

The electrodes are placed at intervals of 10 or 20 percent of the total length of lines created from a system of distances between bony landmarks on the head. This proportional system of positioning electrodes ensures that the relative position of the electrodes on the scalp will be consistent regardless of head size.

For this acquisition, the number of electrodes is 19. Each electrode has a specific notation in which the letters indicate the position of the electrodes on the head: Fp (frontopolar), F (frontal), C (central), T (temporal), P (parietal), O (occipital); while the numbers indicated the hemisphere, odd numbers for the left hemisphere and even numbers over the right hemisphere [72].

4.2. EEG PREPROCESSING AND ARTIFACT DETECTION

Before doing any calculations, EEG data needs to be pre-processed (Figure 18) (Appendix 2). Once the EEG data is uploaded into the MATLAB software, we first need to make sure that we are only working with the data from the 19 scalp electrodes, which are the channels of interest. In some cases, there are more channels that correspond to amplitude testing or the electrocardiogram (ECG) signal, within others. For this, we need to select the rows corresponding to the channels of interest (Figure 19).

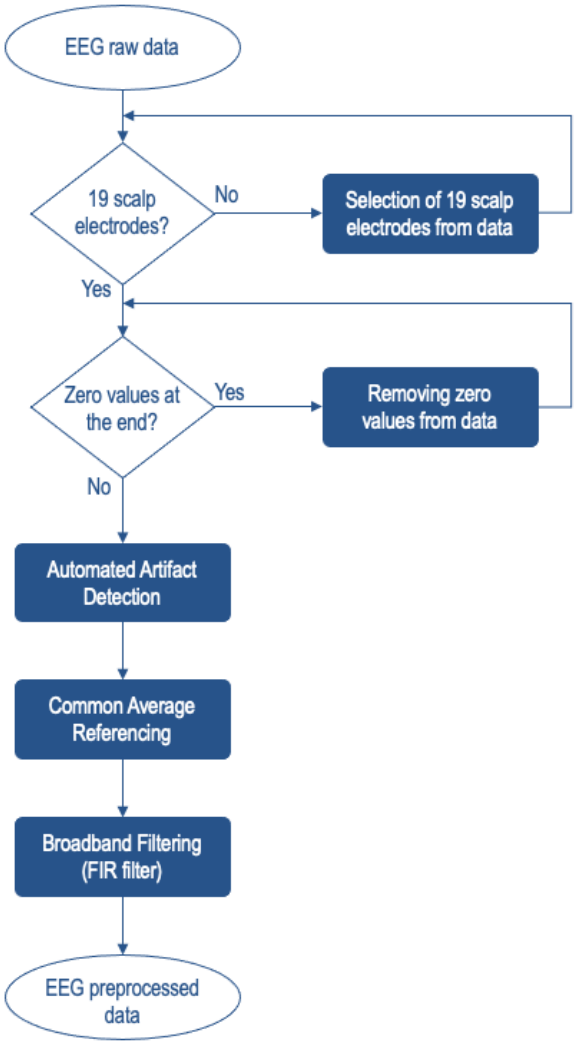

Figure 18 Schematics of the procedures to pre-process EEG data.

Then, the data is filtered using a broadband (1-55 Hz) FIR filter (Figure 19). Although the computational cost of FIR filters is higher compared to IIRs, FIR filters are preferable since they are stable, can be designed with linear phase, avoiding non-linear phase distortions, and are not too computationally expensive for nowadays computers (Appendix 3).

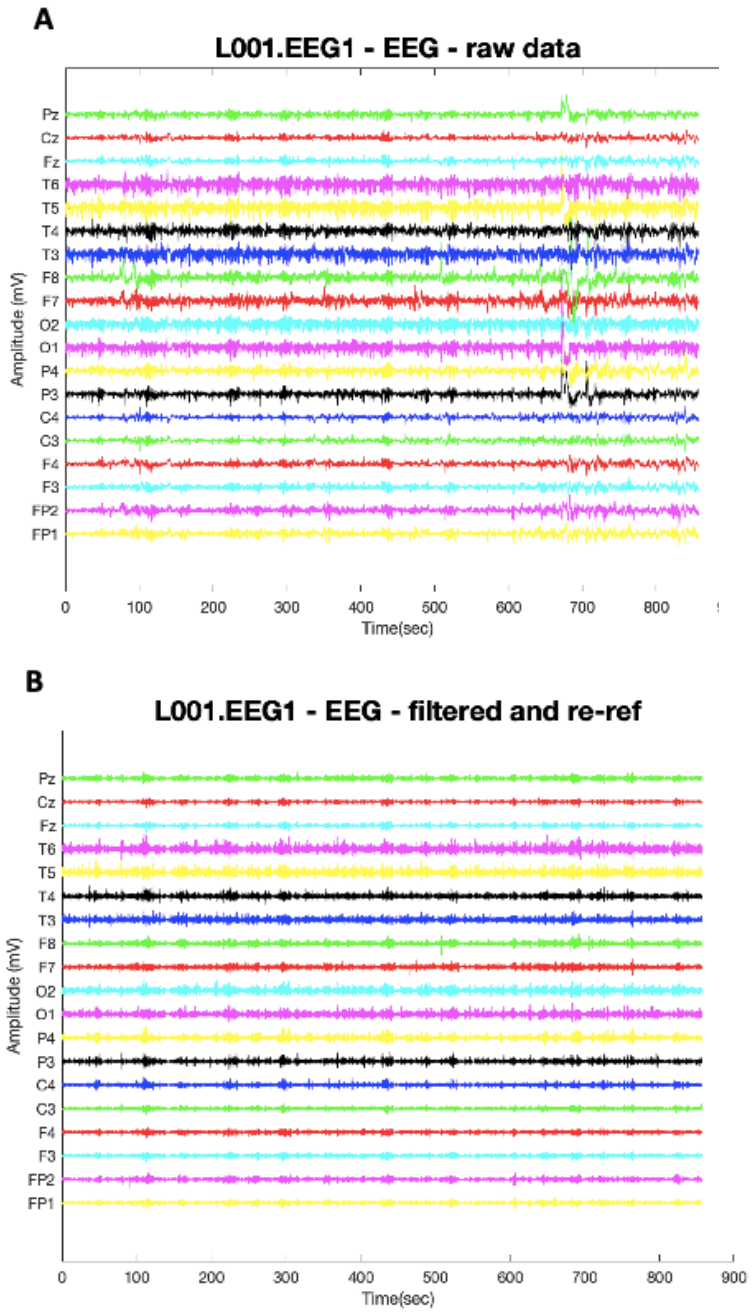

Figure 19 Example case. (A) Plot of raw EEG signal (19 channels) from Subject 01. (B) Plot of re/referenced and filtered EEG signal (19 electrodes) from Subject 01.

Furthermore, time periods of EEG data containing artifacts were identified using an automatic extreme value detection algorithm (Appendix 4) previously described by Smith et al. [2] based on other methods previously published [64], [65]. The inputs of the function are the signal, the sampling frequency (200Hz), a threshold for the standard deviation (7.5), a time buffer (0.9s), and the number of channels involved (1). First, the data is filtered using a broadband bandpass filter. Specifically, a bandpass filter between 1.5 and 40 Hz. Then the mean is subtracted from each channel and the standard deviation is calculated using the entire zero-mean time series. In the cases where the value

of voltage exceeded a threshold of 7.5 standard deviations above the mean value in any of the channels, the time point was marked as an artifact. Furthermore, a buffer of 0.9s is added before and after an extreme amplitude to make sure that the artifacts are fully marked. The output of the automated artifact detector consists of a table in which each row corresponds to one artifact, the first column is the start time of each artifact, and the second column represents the ending time of the corresponding artifact (Figure 20).

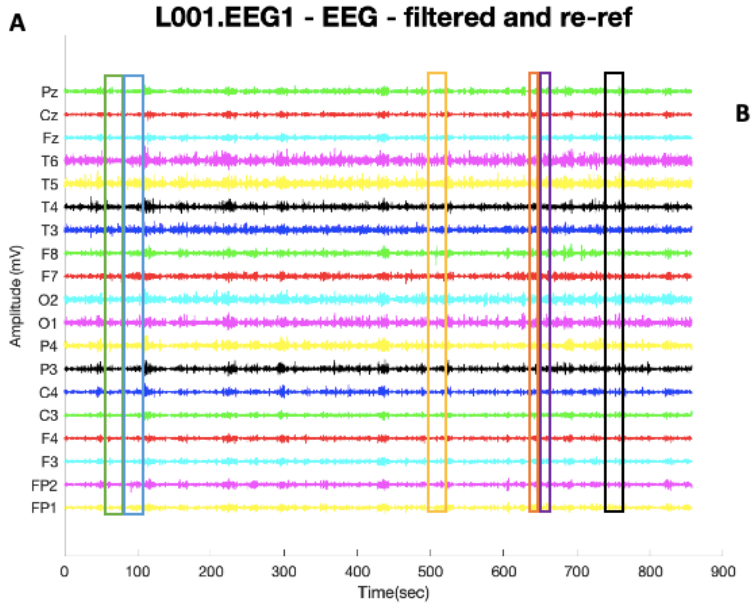

	1	2
1	89.9600	91.7600
2	112.3600	114.1600
3	507.2450	509.2300
4	681.4800	683.8200
5	684.3800	686.4300
6	705.4850	707.5000
7	762.9000	764.7050

Figure 20 Example case. (A) Plot of 19 electrodes of EEG signal from Subject 01 filtered and re/referenced. Colored squares indicated regions where artifacts have been detected. (B) Output of the automated artifact detector. First column representing the start time of an artifact, and the second column representing the corresponding ending time. Colors match the artifacts detected with the corresponding region in the EEG signal.

4.3. CONNECTIVITY CALCULATION AND NETWORK CONSTRUCTION

Functional connectivity networks have been shown to reveal key high-dimensional features of normal and abnormal nervous system physiology. For this reason, they are widely studied in the neuroscience field. Functional connectivity reflects the coupling between regions of the brain that can be anatomically or functionally connected. For this project, we are going to use cross-correlation as the coupling measure. The method used is based on a paper published by Chu et al. in 2012 [61].

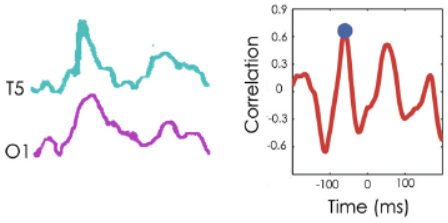

Figure 21 Calculation of the cross-correlation for each 1sec interval for each electrode pair. Example of signals recorded from electrodes T5 and O1 (left) and corresponding maximum absolute values of the correlation (blue dot) [61].

The preprocessed EEG data needs to be divided into 1s windows without artifacts. The data of each window is normalized to have zero mean and unit variance. To calculate cross-correlation, the maximal cross-correlation between all electrode pairs is calculated (Figure 21), allowing a time lag of +/- 200 milliseconds.

For each 1 s window, an undirected binary adjacency matrix M represents the connectivity of the corresponding EEG data. The binary networks generated from each 1 s window is averaged across time to generate weighted functional networks which represent varied epoch lengths. Averaged networks are also created for the entire available recording period for each subject and in each state and frequency band. The value on the connectivity matrix represents the percentage of times each pair had a significant connection in the binary adjacency matrices (Figure 22) (Appendix 5).

For visualization, a connectivity plot is generated where each node represents and electrode, and each edge is weighted according to the values in the total adjacency matrix. To simplify the visualization of the connectivity plot, only the 90th percentile of connections from the connectivity matrix are represented (Figure 22).

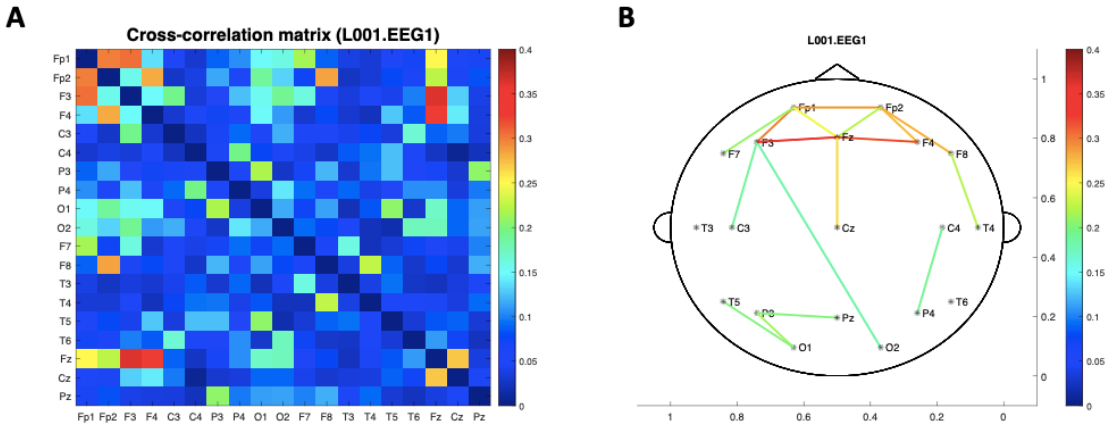

Figure 22 Example of connectivity calculation. (A) Averaged connectivity matrix over all time epochs for subject 01 (Appendix 6). (B) Connectivity plot for the 90th percentile of the connectivity matrix (Appendix 7).

4.4. NETWORK STRENGTH CALCULATION

Two different methodologies will be used to calculate network strength: number of connections above a threshold and mean strength above a percentile.

First, number of connections above a threshold (Figure 23) is performed. For this, we start from the adjacent matrix (19x19) previously obtained. Then, we threshold the matrix, turning into zeros the values of the matrix that are below this threshold, and the values above one will correspond to ones in the new matrix. Then, we will count the number of ones, which will correspond to the number of connections above the threshold. This number corresponds to double the number of strong connections. This is because our matrix is symmetrical. Therefore, we are counting O1-O2 and O2-O1 as two different connections. To solve this problem, we will divide by two the result (Appendix 8).

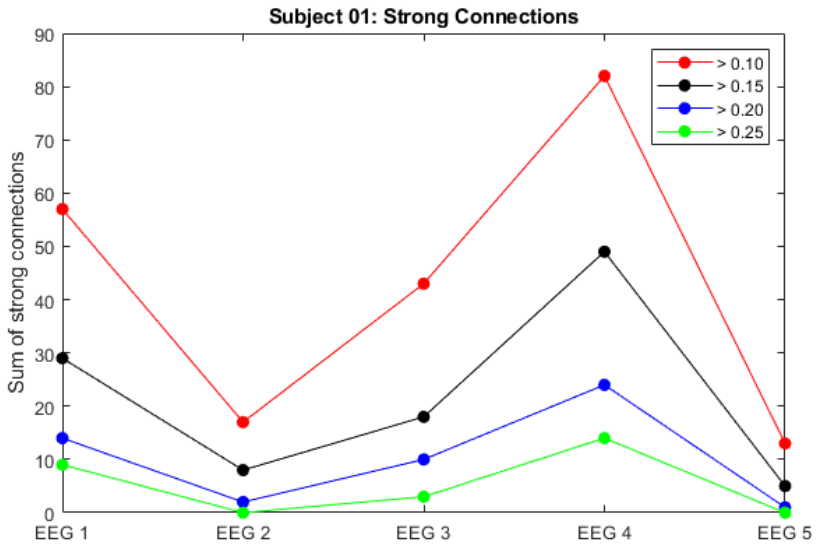

Figure 23 Example plot of the number of strong connections for the 5 EEGs corresponding to Subject 01. Each line corresponds to a different threshold, which are specified in the legend (0.10, 0.15, 0.20, and 0.25).

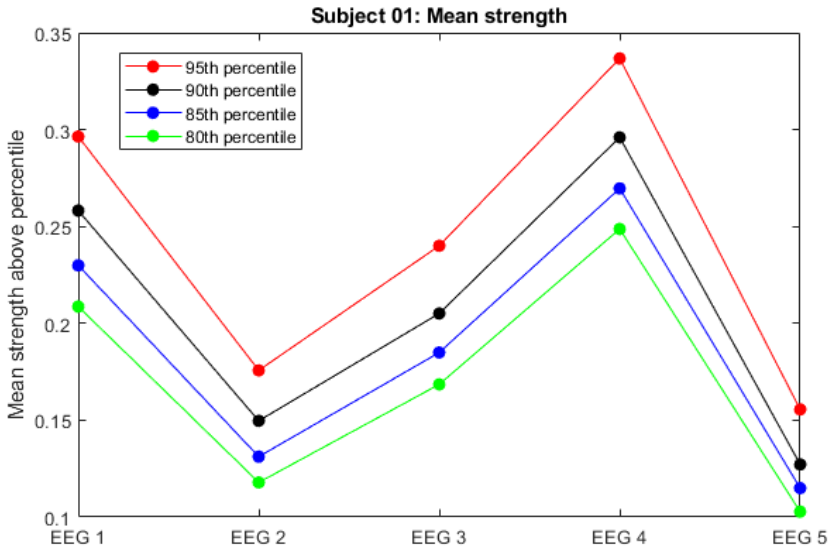

Figure 24 Example plot of mean strength of connections above a percentile threshold for all five EEGs corresponding to Subject 01. Each line corresponds to a different percentile value, which are indicated in the legend (95th, 90th, 85th, and 80th).

Secondly, the mean strength of connections above a percentile (Figure 24) is computed by first finding the percentile threshold and thresholding the matrix. All the values of the adjacency matrix that are below the threshold will be equaled to zero. Then, we will calculate the main of the rest of values (the ones above the threshold (Appendix 9).

5. RESULTS

5.1. FUNCTIONAL CONNECTIVITY TOPOGRAPHIC PLOTS

The main result of this project consists of the functional connectivity plots for each EEG. Each of the patients has a different number of EEGs two of which correspond to the IS and LGS diagnosis times, respectively. Figure 25 corresponds to the EEGs from the first subject. Each EEG corresponds to a recording of the same patient at different points in time. The plots are organized from left to right and from top to bottom. Each EEG was clipped by a neurologist from Children's Hospital of Orange County and a diagnosis was performed. This diagnosis refers to the existence or not of both IS and LGS, and it is written at the top of each connectivity plot, and the different diagnostic options are stated as follows:

- **IS diagnosis**: Infantile Spasms diagnosis.
- **S-/S+:** Infantile Spasms negative/positive.
- **LGS diagnosis:** Lennox-Gastaut Syndrome diagnosis.
- **LGS-/LGS+:** Lennox-Gastaut Syndrome negative/positive.

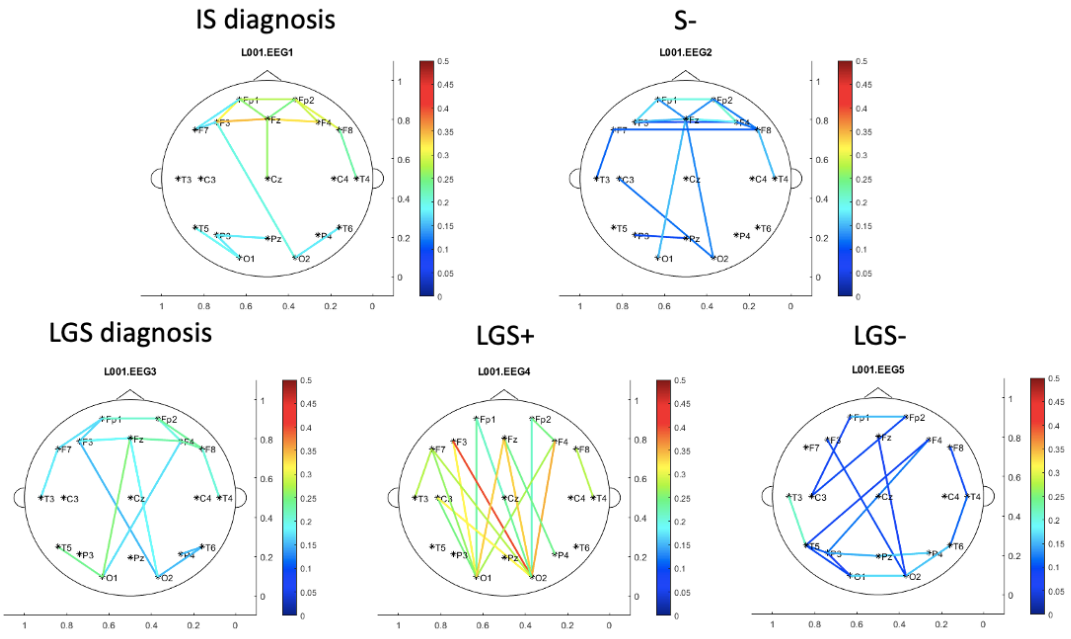

Figure 25 EEG functional connectivity topographic maps or subject 01, who was diagnosed with IS (EEG1), successfully treated (EEG2), and further diagnosed with LGS (EEG3, EEG4), but also successfully treated (EEG5).

In these connectivity plots, we see the representation of the 90th percentile strongest connections. So, as explained before in the project, each line connects to different electrodes and the color is weighted by the strength of the connections. Warmer colors refer to stronger connections, while cooler colors are associated with weaker connections. This connection is mathematically explained as the percentage of one-second windows of the data in which each connection was significant. Therefore, a

connection with a strength value of 1 would mean that this connection was significant in all one-second windows of the data.

If we take a closer look at Figure 25, we can qualitatively analyze subject 1. The first EEG was recorded at the time of IS diagnosis (6 months old), afterwards, the patient was treated, and the spasms were resolved (7 months old). Three months later (10 months old), the child was diagnosed with LGS, which persisted during the following EEG recording (13 months old) but was finally resolved with treatment at 30 months old. By doing a quick look at the plots above, we can notice differences in the connectivity plots. Visually, we can see that in those plots corresponding to IS or LGS state, the connections are stronger. It is important to notice that the number of connections doesn't change, but this is because we are only representing the 10% of stronger connections, so the number of connections will be constant. The connectivity patterns are coherent with the clinicians' diagnosis.

Figure 26 and Figure 27 correspond to subjects 2 and 4, who have similar behavior to subject 1, showing IS diagnosis, followed by positive treatment outcome, LGS diagnosis, and LGS resolution.

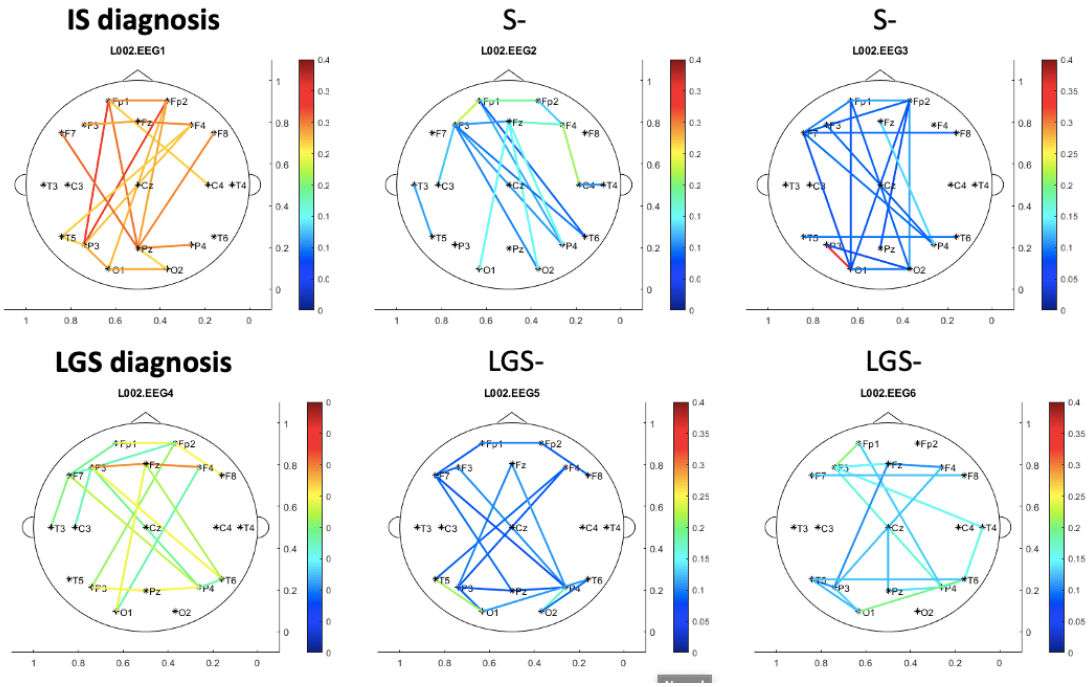

Figure 26 EEG functional connectivity topographic maps or subject 02, who was diagnosed with IS (EEG1), successfully treated (EEG2, EEG3), and further diagnosed with LGS (EEG4), but also successfully treated (EEG5, EEG6).

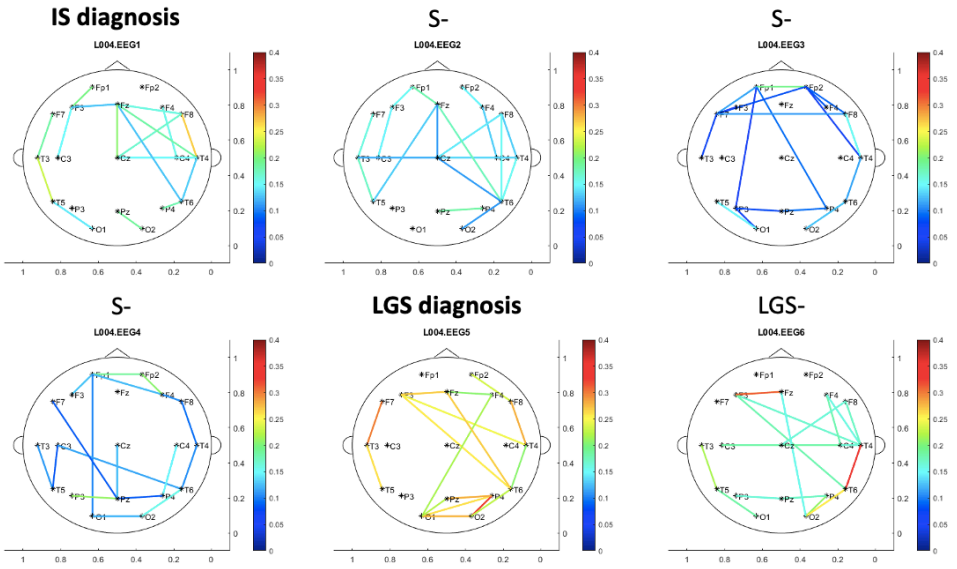

Figure 27 EEG functional connectivity topographic maps or subject 04, who was diagnosed with IS (EEG1), successfully treated (EEG2, EEG3, EEG4), and further diagnosed with LGS (EEG5), but also successfully treated (EEG6).

As another example, we can visually analyze subject 3 (Figure 28). In this case, the child was also diagnosed with IS in the first recording (9 months old), and the following two EEGs showed successful treatment outcomes (9 and 10 months old). Later, the patient was diagnosed with LGS (18 months old), and the last EEG shows a worsening of the disease (22 months old). By looking at these topographic plots, it can be noted how the strength of the connections is still higher during spasms and LGS, while they get lower during IS resolution, which is consistent with what we have seen in subject 1. The main difference between these two subjects is found in the last EEG, where the strength of the connections is still high due to the persistence of LGS.

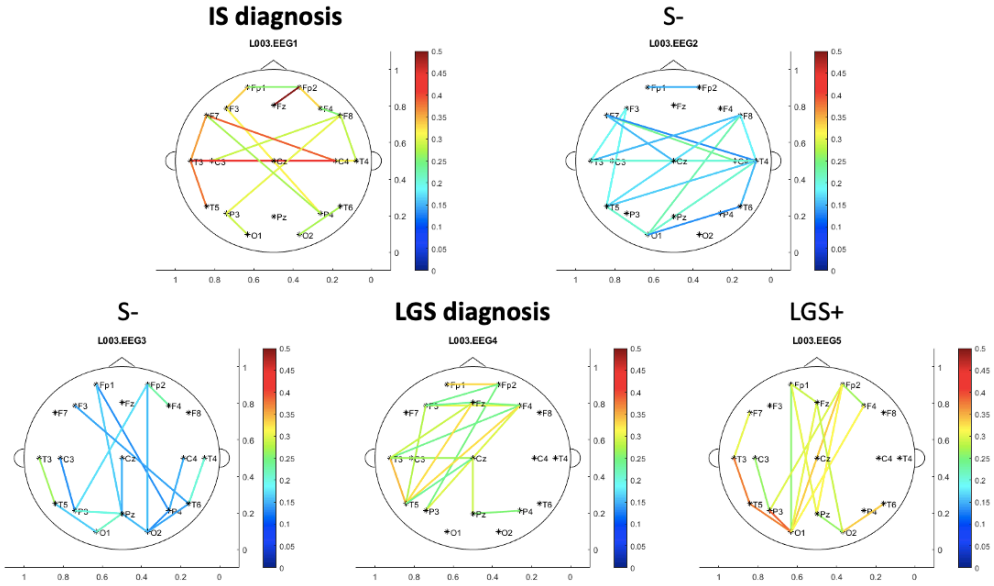

Figure 28 EEG functional connectivity topographic maps or subject 03, who was diagnosed with IS (EEG1), successfully treated (EEG2, EEG 3), and further diagnosed with LGS (EEG4) with a worsening of the disease (EEG5).

Finally, subject 5 (Figure 29) follows a different pattern from the one explained before. After IS diagnosis (32 months), the child has a positive treatment outcome (34 months), but still with a relatively high network, which leads to LGS diagnosis (45 months) and a progressive worsening of the disease (49 and 51 months old). One of the main differences between these subjects and the others is age. This child is much older than the others, and a late diagnosis leads to a poor prognosis.

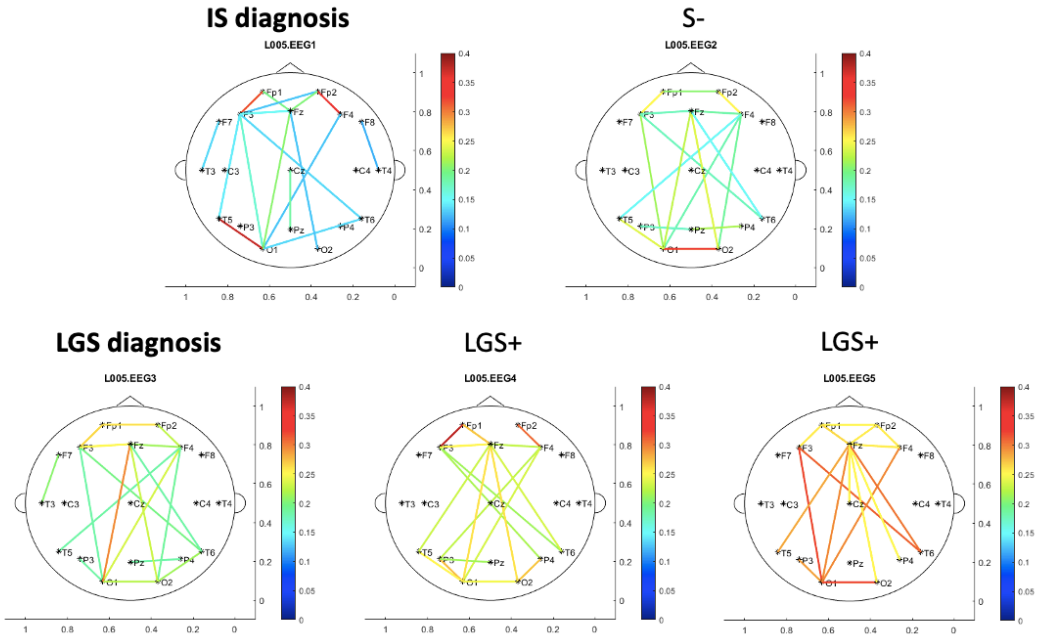

Figure 29 EEG functional connectivity topographic maps or subject 05, who was diagnosed with IS (EEG1), successfully treated (EEG2), and further diagnosed with LGS (EEG3) with a worsening of the disease (EEG4, EEG5).

5.2. CONNECTIVITY VS. DIAGNOSIS

The number of strong connections above a threshold of 0.1 was calculated for each EEG to quantify the overall strength of the networks. Figure 30 shows the evolution of this parameter for each EEG of the patients. Therefore, each patient corresponds to a line plot (identified by colors in the legend). Further, the markers represent the diagnosis where the circles refer to IS and the starts to LGS. Further, when a marker is filled, it means that the diagnosis (IS or LGS) was positive, while a non-filled marker refers to a negative diagnosis, therefore an improvement of the subject.

If we analyze the plot of our case study (Figure 30), we can identify several trends. The first plot corresponds to the time of IS diagnosis (filled circle marker) for all the patients. Then, the second time point is a non-filled circle for all the subjects, which indicates a positive treatment outcome and IS recovery. In this transition, we can clearly identify a decreasing trend of number of strong connections above a threshold of 0.1. From here, subjects have a different amount of 'normal' EEG recording that tend to have a low number of strong connections.

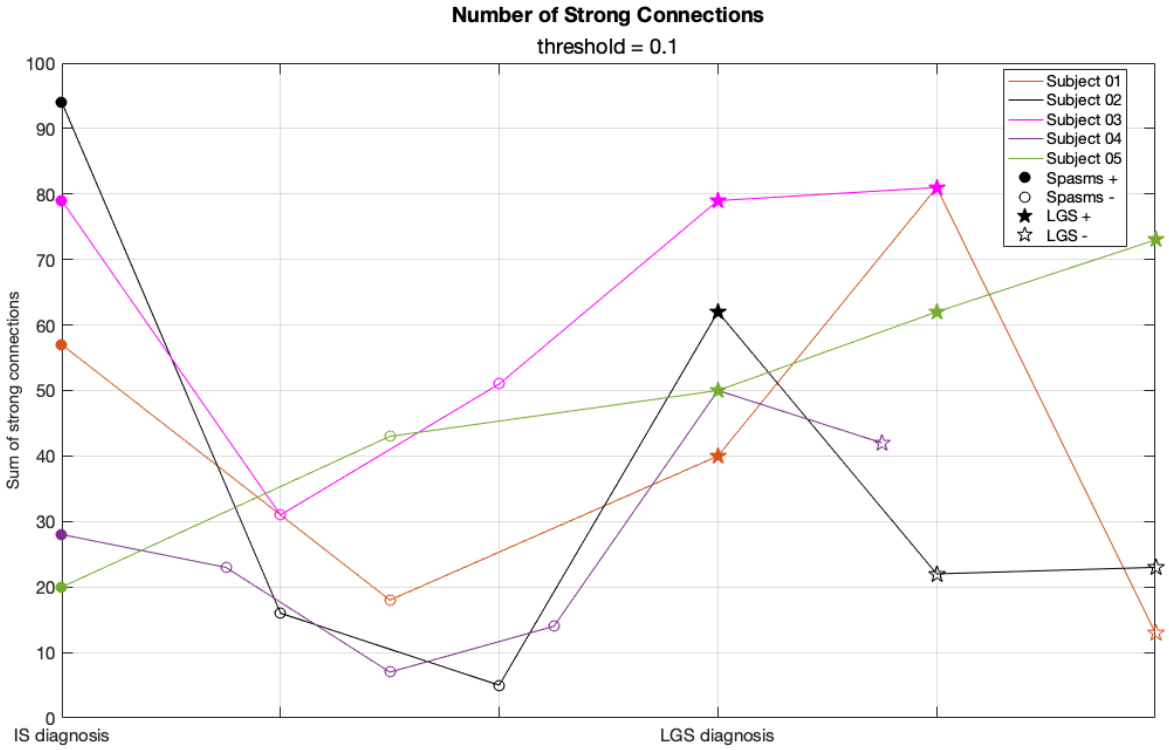

Figure 30 Number of strong connections with threshold 0.1 in IS patients that progressed to LGS. The time-points are normalized at the times of IS and LGS diagnosis. The markers refer to IS (circle) and LGS (star) where a filled marker corresponds to a positive diagnosis and a non-filled marker to a negative diagnosis.

Afterward, all subjects are diagnosed with LGS (filled star marker), and the number of strong connections shows an increasing trend. After LGS diagnosis, we could divide the subjects in two groups:

- Subjects 2 and 4 show a positive treatment outcome, therefore, LGS remission. This diagnosis is accompanied by a decrease in the number of strong connections.
- Subjects 1, 3, and 5 show continuing LGS diagnosis and a worsening of the disease. This is demonstrated by an increase of the number of strong connections. Subject number 1 has a third EEG recording in which clinicians declare a remission of LGS, which is accompanied by a decrease in the number of strong connections.

Further, the mean strength of connections above the 90th percentile is computed. We hypothesized that this result would be equivalent to the number of strong connections, and Figure 31 proves this hypothesis was true. The results obtained are not exactly equal to Figure 31, but they are strongly equivalent. Again, we find an increasing trend at the time of a diagnosis, a decrease after positive treatment outcome and/or epilepsy resolution, and an increase of mean strength associated with a worsening of the disease.

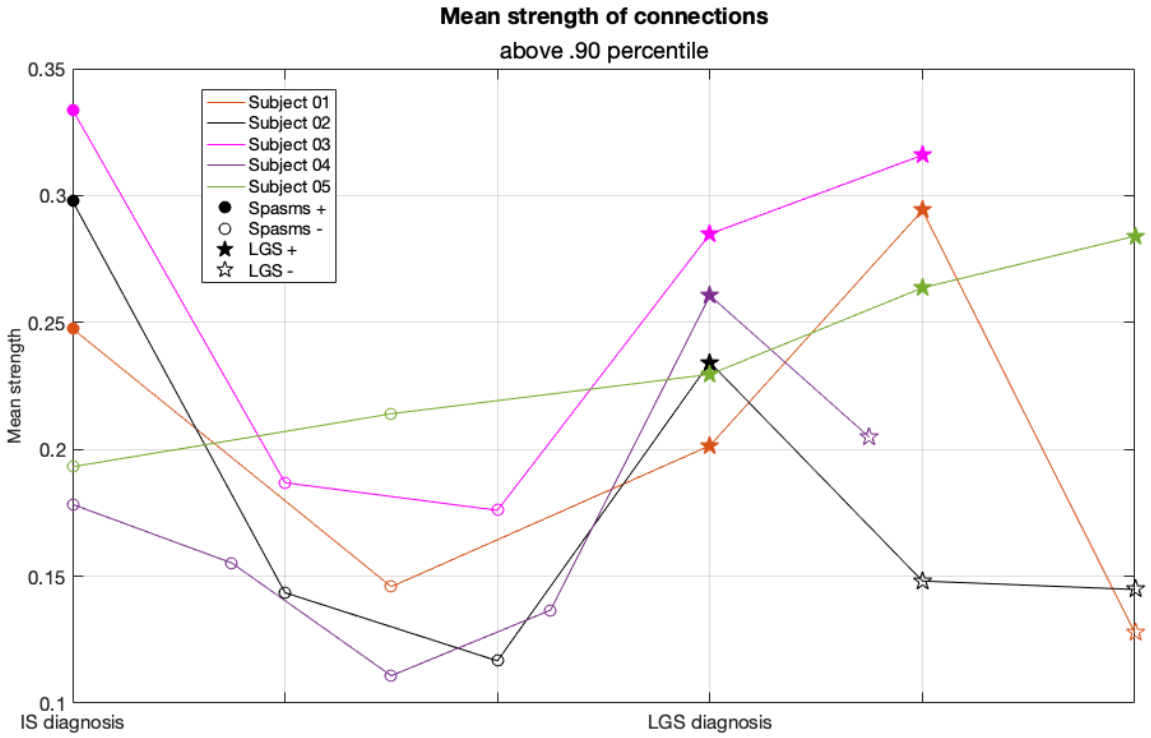

Figure 31 Mean strength of connections above the 90th percentile in IS patients that progressed to LGS. The time-points are normalized at the times of IS and LGS diagnosis. The markers refer to IS (circle) and LGS (star) where a filled marker corresponds to a positive diagnosis and a non-filled marker to a negative diagnosis.

5.3. CONNECTIVITY VS. AGE

During physiological growth, the brain of children undergoes a series of normal changes to allow is correct development. Therefore, it could be stated that the changes seen in the previous results could be caused by the aging of the subjects. To prove this wrong, we plotted both the number of strong connections above a 0.1 threshold and the mean strength of connections above the 90th percentile as a function of the children's age. Figure 32 and Figure 33 show the distribution of the two variables previously studied as a function of the subjects' age, respectively. Both plots show that there is no correlation between the two variables and age, which demonstrates that the evolution of the functional connectivity of the subjects' brains is due to the progression of the epilepsies.

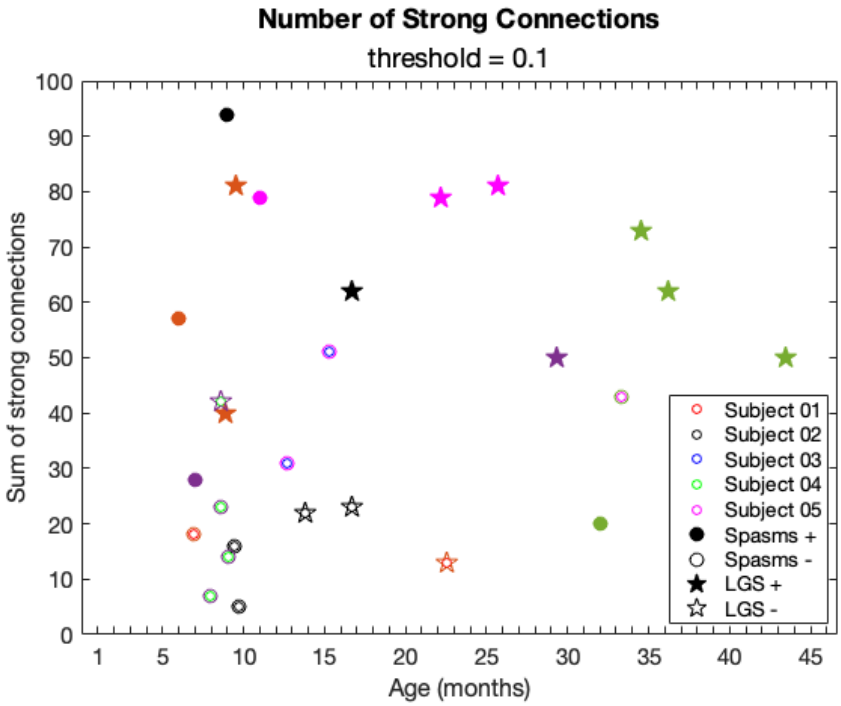

Figure 32 Number of strong connections above a percentile of 0.1 in IS patients that progressed to LGS as a function of the children's age. Each color represents a subject and the markers correspond to the diagnosis (explained in more detail in the legend).

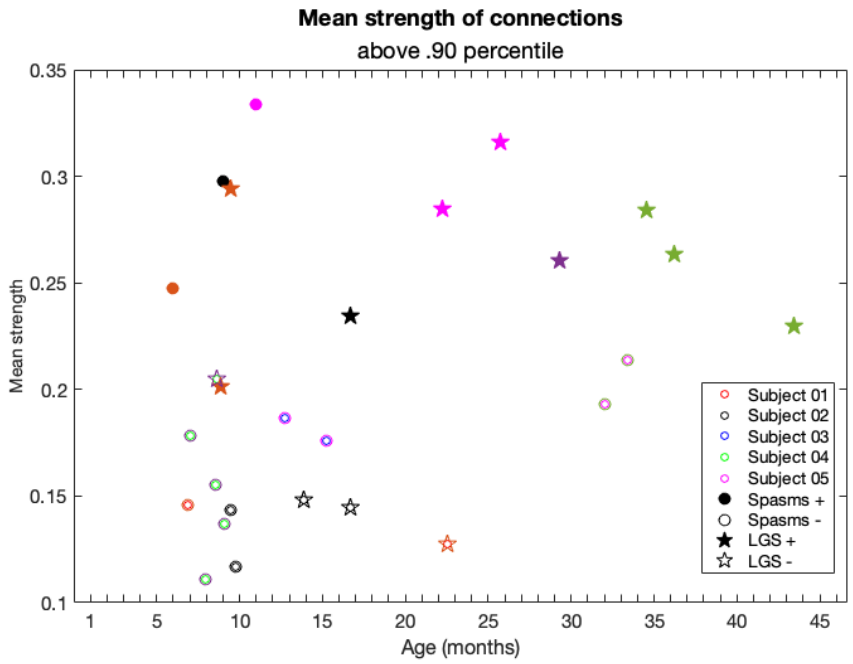

Figure 33 Mean strength of connections above the 90th percentile in IS patients that progressed to LGS as a function of the children's age. Each color represents a subject and the markers correspond to the diagnosis (explained in more detail in the legend).

6. TIMELINE & BUDGET

A GANTT diagram (Figure 34). was used to keep track of the timeline of the project. The total real-time invested in this project was for months, from February to June. All the tasks reflected by the GANTT were done by one person and they are organized similarly to the index of this thesis.

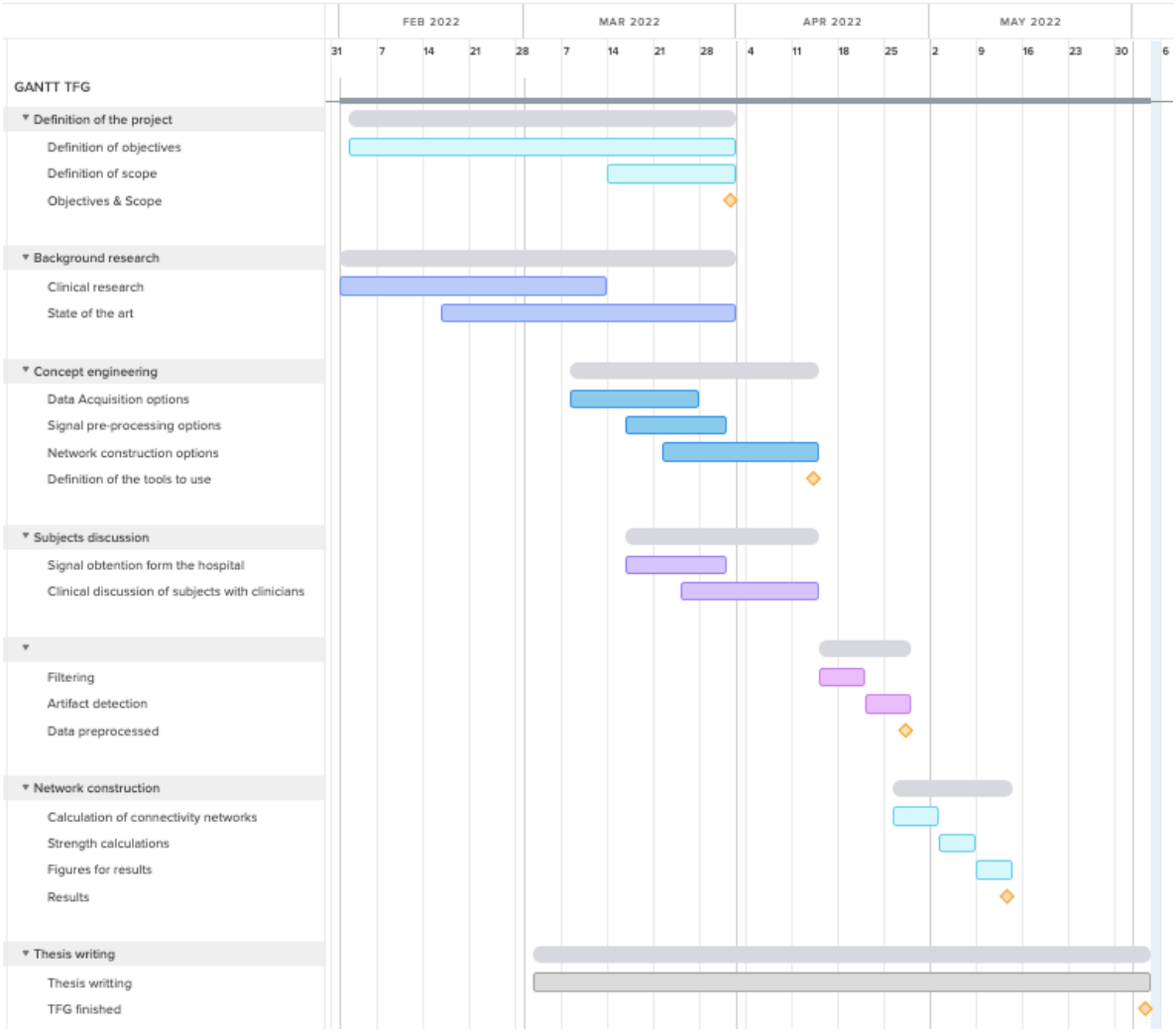

Figure 34 GANTT of the Project. The column on the left shows the tasks performed, and the time at which they were done is highlighted in different colors on the right.

The first task consisted of acquiring knowledge about the field. The field of this project is very specific, and it was very unknown to me before starting. Therefore, the first step was to do research on the two pathologies I was going to study: Infantile Spasms, and Lennox-Gastaut Syndrome. Also, exhaustive research was done on the computational analysis that had been done by other research groups to characterize the features and biomarkers of both epilepsies and, also, the progression of IS to LGS. All this research allowed us to understand the state of the art and the needs in the field, being able to define the objectives and scope of the research project.

Parallel to the background research, we started to analyze the different options available to acquire the data, pre-process the signals, and build the networks of interest. Once we decide all the tools that were going to be needed, the Children's Hospital of Orange County had already sent us the data. Before working with it, it was important to be aware the specific case of each subject, to further understand the results. For this, we met with the neurologists from CHOC Hospital.

The last step was to work with the data. The steps followed, in order, were the pre-processing – with both the filtering and the artifacts detection, the network construction, and the strength calculations. Once we had all the results it was necessary to make figures that would show our results in a coherent and efficient way. The writing of the thesis was done is parallel with all the tasks performed.

	Name of product	Cost (per unit)	Units	Total cost (per product)
	Precision 5820 Tower Workstation [73]	$2,529.00	1	$2,529.00
	Dell 24 Monitor - S2421HSX [74]	$209.99	2	$419.98
	Dell Pro Wireless Keyboard and Mouse – KM5221W [75]	$47.99	1	$47.99
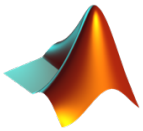	MATLAB annual license [76]	$880 / 1-year	6 months	$440
			Total cost	**$3436.97**

Table 3 Budget of the material costs, which include a full Workstation and the MATLAB license for 6 months.

For the budget, we need to differentiate between material and personal expenses. For this project, the only material needed is a full workstation – including a tower, two monitors, a keyboard, and a mouse –, and a license for the software MATLAB for 6 months. The MATLAB licenses can only be purchased perpetual or annual. The University of California Irvine has a perpetual license, but for

the sake of this budget, we will calculate the price of having the license for 6 months, dividing by two the annual price. We could consider adding the EEG recording system, but it is important to note that the signals are not obtained for research. Contrarily, these EEG recordings are obtained as a routine procedure for epileptic infants, and some of them are sent later to our research group to study them. An approximate budget for the workstation is shown in Table 3.

Secondly, we need to consider the budget for personal resources. In this case, it was just me working in the project for 6 months. I was considered a Step 5 research student (see Figure 35), and the typical appointment is at 49% of the total salary. The annual salary at Step 5 is $60,599, so a 6-month appointment at 49% would be 60,599*0.5*0.49 = $14,846.76. Further, the tuition and fees for two quarters need to be included. Right now, tuition and fees for students that are non-California residents are $11,046.32 per quarter. These sums up to a total of $36,939.40 for personal resources.

Considering both material and personal costs, the project needed a budget of $40,376.37, which translate to 37,550.02€ - considering a conversion factor of 0.93. It is important to remark that the workstation was not purchased exclusively for this project, as well as the MATLAB license. Further, as a researcher, I was working on more than one project, not only this one. So, realistically, the costs of the project would be lower.

GRADUATE STUDENT RESEARCHER
FISCAL YEAR RATES
Salary Admin Plan: T022

		Adjusted Scale 10/1/2020			Adjusted Scale* 10/1/2021		
Rank	Step	Annual	Monthly	Hourly	Annual	Monthly	Hourly
GRADUATE STUDENT RESEARCHER Grade IV (e.g., 003284, 003282, 003266)	I	42,729	3,560.75	20.46	44,011	3,667.58	21.08
	II	46,053	3,837.75	22.06	47,435	3,952.92	22.72
	III	51,072	4,256.00	24.46	52,604	4,383.67	25.19
	IV	55,163	4,596.92	26.42	56,818	4,734.83	27.21
	V	58,834	4,902.83	28.18	60,599	5,049.92	29.02
	VI	61,565	5,130.42	29.49	63,412	5,284.33	30.37
	VII	66,497	5,541.42	31.85	68,492	5,707.67	32.80
	VIII	71,787	5,982.25	34.38	73,941	6,161.75	35.41
	IX	77,547	6,462.25	37.14	79,873	6,656.08	38.25
	X	83,727	6,977.25	40.10	86,239	7,186.58	41.30
GRADUATE STUDENT ASSISTANT RESEARCHER Grade II (e.g., 003274, 003273)	I	42,729	3,560.75	20.46	44,011	3,667.58	21.08
	II	48,797	4,066.42	23.37	50,261	4,188.42	24.07

*The 3 percent increase is applied on the montly rate (rounded to the nearest dollar) and deriving annual rates based on the rounded monthly rate. Please note that this **new calculation does not change the monhtly or hourly rates**.

Figure 35 Graduates student researcher fiscal year rates. Salary Admin Plan: T022.

7. CONCLUSIONS

Throughout this project, we have been able to meet all the goals we set in the beginning. The main aim of the study was to evaluate the EEG-based functional connectivity of subjects during the progression from Infantile Spasms (IS) to Lennox-Gastaut Syndrome (LGS). But before, we needed to reach smaller targets.

Firstly, we preprocessed the scalp EEG data by using a broadband FIR filter from 1 to 55 Hz. Also, we detected the artifacts by using an amplitude-based automatic artifact detector to increase the signal-to-noise ratio and ensure a correct interpretation of the data.

Secondly, we built the functional networks by using a computational tool called cross-correlation in which the correlation between electrode pairs is assessed in 1-second windows. Further, the significance of the results was determined by applying permutation resampling to the cross-correlation calculations.

Finally, we have been able to answer our initial question and prove our hypothesis. Overall, functional connectivity strength reflected the presence of IS, as well as a positive response to treatment. IS diagnosis was associated with high strength, while a resolution of spasms after treatment produced a decrease in the connectivity strength. Further, LGS diagnosis was also linked to an increase in strength. After LGS treatment, children could be divided into two groups. On one hand, subjects exhibited a decrease in the connectivity strength after a positive treatment outcome, while worsening of the disease was associated with maintenance or increase of the connectivity. Therefore, functional connectivity could be used as a biomarker to improve LGS diagnosis in patients with an IS history, improving their prognosis.

As future work, it is critical to extend this analysis to a larger cohort of subjects to increase the power of the study and validate these results. The subjects we are working with need to fulfill a specific series of characteristics. Therefore, the number of patients under study is usually a limitation. However, it is important to increase the number of subjects to avoid variations in the results due to the specific etiology of each child.

8. BIBLIOGRAPHY

[1] J. E. Piña-Garza et al., "Assessment of treatment patterns and healthcare costs associated with probable Lennox–Gastaut syndrome," Epilepsy and Behavior, vol. 73, pp. 46–50, 2017, doi: 10.1016/j.yebeh.2017.05.021.

[2] R. J. Smith, D. K. Hu, D. W. Shrey, R. Rajaraman, S. A. Hussain, and B. A. Lopour, "Computational characteristics of interictal EEG as objective markers of epileptic spasms," Epilepsy Research, vol. 176, no. January, p. 106704, 2021, doi: 10.1016/j.eplepsyres.2021.106704.

[3] W. Stacey et al., "Emerging roles of network analysis for epilepsy," Epilepsy Research, vol. 159, no. December 2019, p. 106255, 2020, doi: 10.1016/j.eplepsyres.2019.106255.

[4] P. Pavone, P. Striano, R. Falsaperla, L. Pavone, and M. Ruggieri, "Infantile spasms syndrome, West syndrome and related phenotypes: What we know in 2013," Brain and Development, vol. 36, no. 9, pp. 739–751, 2014, doi: 10.1016/j.braindev.2013.10.008.

[5] I. L. Goldsmith, M. L. Zupanc, and J. R. Buchhalter, "Long-term seizure outcome in 74 patients with Lennox-Gastaut syndrome: Effects of incorporating MRI head imaging in defining the cryptogenic subgroup," Epilepsia, vol. 41, no. 4, pp. 395–399, 2000, doi: 10.1111/j.1528-1157.2000.tb00179.x.

[6] M. Wong and E. Trevathan, "Infantile spasms," Pediatric Neurology, vol. 24, no. 2, pp. 89–98, 2001, doi: 10.1016/S0887-8994(00)00238-1.

[7] F. A. Gibbs and E. L. Gibbs, Atlas of Electroencephalography, Vol.2, Epilepsy, Addison-Wesley, Cambridge, MA. 1952.

[8] S. A. Hussain et al., "Hypsarrhythmia assessment exhibits poor interrater reliability: A threat to clinical trial validity," Epilepsia, vol. 56, no. 1, pp. 77–81, 2015, doi: 10.1111/epi.12861.

[9] E. Trevathan, C. C. Murphy, and M. Yeargin-Allsopp, "The descriptive epidemiology of infantile spasms among Atlanta children," Epilepsia, vol. 40, no. 6, pp. 748–751, 1999, doi: 10.1111/j.1528-1157.1999.tb00773.x.

[10] J. F. Donat and F. S. Wright, "Seizures in Series: Similarities Between Seizures of the West and Lennox-Gastaut Syndromes," Epilepsia, vol. 32, no. 4, pp. 504–509, 1991, doi: 10.1111/j.1528-1157.1991.tb04684.x.

[11] H. Rantala and T. Putkonen, "Occurrence, outcome, and prognostic factors of infantile spasms and Lennox-Gastaut syndrome," Epilepsia, vol. 40, no. 3, pp. 286–289, 1999, doi: 10.1111/j.1528-1157.1999.tb00705.x.

[12] J. S. Archer, A. E. L. Warren, G. D. Jackson, and D. F. Abbott, "Conceptualizing Lennox-Gastaut Syndrome as a Secondary Network Epilepsy," Frontiers in Neurology, vol. 5, no. October, pp. 1–11, 2014, doi: 10.3389/fneur.2014.00225.

[13] A. A. Asadi-pooya, "LGS a comprehensive review vv.pdf," pp. 403–414, 2018.

[14] E. Trevathan, C. C. Murphy, and M. Yeargin-Allsopp, "Prevalence and descriptive epidemiology of Lennox-Gastaut syndrome among Atlanta children," Epilepsia, vol. 38, no. 12, pp. 1283–1288, 1997, doi: 10.1111/j.1528-1157.1997.tb00065.x.

[15] A. A. Asadi-Pooya and M. Sharifzade, "Lennox-Gastaut syndrome in south Iran: Electro-clinical manifestations," Seizure, vol. 21, no. 10, pp. 760–763, 2012, doi: 10.1016/j.seizure.2012.08.003.

[16] P. R. Camfield, "Definition and natural history of Lennox-Gastaut syndrome," Epilepsia, vol. 52, no. SUPPL. 5, pp. 3–9, 2011, doi: 10.1111/j.1528-1167.2011.03177.x.

[17] G. R. Müller-Putz, "Electroencephalography," Handbook of Clinical Neurology, vol. 168, no. 2007, pp. 249–262, 2020, doi: 10.1016/B978-0-444-63934-9.00018-4.

[18] "The Pediatric EEG." https://www.learningeeg.com/pediatric (accessed Jun. 05, 2022).

[19] M. Abo-Zahhad, S. M. Ahmed, and S. N. Abbas, "A New EEG Acquisition Protocol for Biometric Identification Using Eye Blinking Signals," International Journal of Intelligent Systems and Applications, vol. 7, no. 6, pp. 48–54, May 2015, doi: 10.5815/ijisa.2015.06.05.

[20] S. T. Demarest et al., "The impact of hypsarrhythmia on infantile spasms treatment response: Observational cohort study from the National Infantile Spasms Consortium," Physiol Behav, vol. 176, no. 5, pp. 139–148, 2017, doi: 10.1111/epi.13937.The.

[21] J. Y. Wu, S. Koh, R. Sankar, and G. W. Mathern, "Paroxysmal fast activity: An interictal scalp EEG marker of epileptogenesis in children," Epilepsy Research, vol. 82, no. 1, pp. 99–106, 2008, doi: 10.1016/j.eplepsyres.2008.07.010.

[22] J. R. Mytinger et al., "Improving the inter-rater agreement of hypsarrhythmia using a simplified EEG grading scale for children with infantile spasms," Epilepsy Research, vol. 116, pp. 93–98, 2015, doi: 10.1016/j.eplepsyres.2015.07.008.

[23] J. R. Mytinger, J. Vidaurre, M. Moore-Clingenpeel, J. R. Stanek, and D. V. F. Albert, "A reliable interictal EEG grading scale for children with infantile spasms – The 2021 BASED score," Epilepsy Research, vol. 173, p. 106631, 2021, doi: 10.1016/j.eplepsyres.2021.106631.

[24] D. K. Hu, A. Mower, D. W. Shrey, and B. A. Lopour, "Effect of interictal epileptiform discharges on EEG-based functional connectivity networks," Clinical Neurophysiology, vol. 131, no. 5, pp. 1087–1098, 2020, doi: 10.1016/j.clinph.2020.02.014.

[25] P. E. Davis et al., "Increased electroencephalography connectivity precedes epileptic spasm onset in infants with tuberous sclerosis complex," Natural Products as Platforms To Overcome Antibiotic Resistance Sean, vol. 176, no. 3, pp. 139–148, 2017, doi: 10.1111/epi.16284.Increased.

[26] E. van Diessen, W. M. Otte, C. J. Stam, K. P. J. Braun, and F. E. Jansen, "Electroencephalography based functional networks in newly diagnosed childhood epilepsies," Clinical Neurophysiology, vol. 127, no. 6, pp. 2325–2332, 2016, doi: 10.1016/j.clinph.2016.03.015.

[27] H. Suzuki et al., "Epileptogenic modulation index and synchronization in hypsarrhythmia of West syndrome secondary to perinatal arterial ischemic stroke," Clinical Neurophysiology, vol. 132, no. 5, pp. 1185–1193, 2021, doi: 10.1016/j.clinph.2020.12.028.

[28] S. A. Burroughs, R. P. Morse, S. H. Mott, and G. L. Holmes, "Brain connectivity in West syndrome," Seizure, vol. 23, no. 7, pp. 576–579, 2014, doi: 10.1016/j.seizure.2014.03.016.

[29] N. Japaridze et al., "Neuronal networks in west syndrome as revealed by source analysis and renormalized partial directed coherence," Brain Topography, vol. 26, no. 1, pp. 157–170, 2013, doi: 10.1007/s10548-012-0245-y.

[30] V. Nenadovic, R. Whitney, J. Boulet, and M. A. Cortez, "Hypsarrhythmia in epileptic spasms: Synchrony in chaos," Seizure, vol. 58, pp. 55–61, 2018, doi: 10.1016/j.seizure.2018.03.026.

[31] R. J. Smith, D. W. Shrey, S. A. Hussain, and B. A. Lopour, "Quantitative Characteristics of Hypsarrhythmia in Infantile Spasms," Proceedings of the Annual International Conference of the IEEE Engineering in Medicine and Biology Society, EMBS, vol. 2018-July, pp. 538–541, 2018, doi: 10.1109/EMBC.2018.8512348.

[32] K. Kobayashi et al., "Complex observation of scalp fast (40–150 Hz) oscillations in West syndrome and related disorders with structural brain pathology," Epilepsia Open, vol. 2, no. 2, pp. 260–266, 2017, doi: 10.1002/epi4.12043.

[33] K. Kobayashi, T. Akiyama, M. Oka, F. Endoh, and H. Yoshinaga, "A storm of fast (40-150Hz) oscillations hypsarrhythmia in West syndrome," Annals of Neurology, vol. 77, no. 1, pp. 58–67, 2015, doi: 10.1002/ana.24299.

[34] H. Tsuchiya, F. Endoh, T. Akiyama, M. Matsuhashi, and K. Kobayashi, "Longitudinal correspondence of epilepsy and scalp EEG fast (40–200 Hz) oscillations in pediatric patients with tuberous sclerosis complex," Brain and Development, vol. 42, no. 9, pp. 663–674, 2020, doi: 10.1016/j.braindev.2020.06.001.

[35] C. M. McCrimmon et al., "Automated detection of ripple oscillations in long-term scalp EEG from patients with infantile spasms," Journal of Neural Engineering, vol. 18, no. 1, 2021, doi: 10.1088/1741-2552/abcc7e.

[36] H. Nariai et al., "Scalp EEG interictal high frequency oscillations as an objective biomarker of infantile spasms," Clinical Neurophysiology, vol. 131, no. 11, pp. 2527–2536, 2020, doi: 10.1016/j.clinph.2020.08.013.

[37] L. Yan, L. Li, J. Chen, L. Wang, L. Jiang, and Y. Hu, "Application of High-Frequency Oscillations on Scalp EEG in Infant Spasm: A Prospective Controlled Study," Frontiers in Human Neuroscience, vol. 15, no. June, pp. 1–10, 2021, doi: 10.3389/fnhum.2021.682011.

[38] Y. Iwatani et al., "Ictal high-frequency oscillations on scalp EEG recordings in symptomatic West syndrome," Epilepsy Research, vol. 102, no. 1–2, pp. 60–70, 2012, doi: 10.1016/j.eplepsyres.2012.04.020.

[39] A. L. Lux and J. P. Osborne, "A proposal for case definitions and outcome measures in studies of infantile spasms and West syndrome: Consensus statement of the West Delphi Group," Epilepsia, vol. 45, no. 11, pp. 1416–1428, 2004, doi: 10.1111/j.0013-9580.2004.02404.x.

[40] D. W. Shrey, O. Kim McManus, R. Rajaraman, H. Ombao, S. A. Hussain, and B. A. Lopour, "Strength and stability of EEG functional connectivity predict treatment response in infants with epileptic spasms," Clinical Neurophysiology, vol. 129, no. 10, pp. 2137–2148, 2018, doi: 10.1016/j.clinph.2018.07.017.

[41] A. Tanritanir, S. Vieluf, S. Jafarpour, X. Wang, and T. Loddenkemper, "EEG Biomarkers of Repository Corticotropin Injection Treatment," Journal of Clinical Neurophysiology, vol. Publish Ah, no. 00, pp. 1–8, 2021, doi: 10.1097/wnp.0000000000000886.

[42] W. Wang et al., "Automatic detection of interictal ripples on scalp EEG to evaluate the effect and prognosis of ACTH therapy in patients with infantile spasms," Epilepsia, vol. 62, no. 9, pp. 2240–2251, 2021, doi: 10.1111/epi.17018.

[43] L. Wan et al., "Assessing Risk for Relapse among Children with Infantile Spasms Using the Based Score after ACTH Treatment: A Retrospective Study," Neurology and Therapy, 2022, doi: 10.1007/s40120-022-00347-7.

[44] K. Yamada et al., "Predictive value of EEG findings at control of epileptic spasms for seizure relapse in patients with West syndrome," Seizure, vol. 23, no. 9, pp. 703–707, 2014, doi: 10.1016/j.seizure.2014.05.010.

[45] J. G. Millichap and J. J. Millichap, "Prediction of Infantile Spasms Recurrence after ACTH Therapy," Pediatric Neurology Briefs, vol. 29, no. 12, p. 93, 2015, doi: 10.15844/pedneurbriefs-29-12-4.

[46] D. Bernardo, H. Nariai, S. A. Hussain, R. Sankar, and J. Y. Wu, "Interictal scalp fast ripple occurrence and high frequency oscillation slow wave coupling in epileptic spasms," Clinical Neurophysiology, vol. 131, no. 7, pp. 1433–1443, 2020, doi: 10.1016/j.clinph.2020.03.025.

[47] Y. J. Chu, C. F. Chang, W. C. Weng, P. C. Fan, J. S. Shieh, and W. T. Lee, "Electroencephalography complexity in infantile spasms and its association with treatment response," Clinical Neurophysiology, vol. 132, no. 2, pp. 480–486, 2020, doi: 10.1016/j.clinph.2020.12.006.

[48] J. A. Nelson, S. Demarest, J. Thomas, E. Juarez-Colunga, and K. G. Knupp, "Evolution of Infantile Spasms to Lennox-Gastaut Syndrome: What Is There to Know?," Journal of Child Neurology, vol. 36, no. 9, pp. 752–759, Aug. 2021, doi: 10.1177/08830738211000514.

[49] A. Calvo, M. C. Buompadre, A. Gallo, R. Gutiérrez, G. R. Valenzuela, and R. Caraballo, "Electroclinical pattern in the transition from West to Lennox-Gastaut syndrome," Epilepsy Research, vol. 167, Nov. 2020, doi: 10.1016/j.eplepsyres.2020.106446.

[50] S. J. You, H. D. Kim, and H. C. Kang, "Factors Influencing the Evolution of West Syndrome to Lennox-Gastaut Syndrome," Pediatric Neurology, vol. 41, no. 2, pp. 111–113, Aug. 2009, doi: 10.1016/j.pediatrneurol.2009.03.006.

[51] Jorge Malagon Valdez, "• Risk factors for development of LGS were developmental delay and seizures prior to the onset of IS and poor response to first treatment for IS.".

[52] G. R. Müller-Putz, "Electroencephalography," Handbook of Clinical Neurology, vol. 168, no. 2007, pp. 249–262, 2020, doi: 10.1016/B978-0-444-63934-9.00018-4.

[53] T. Mima and M. Hallett, "Electroencephalographic analysis of cortico-muscular coherence: reference effect, volume conduction and generator mechanism," Clinical Neurophysiology, vol. 110, no. 11, pp. 1892–1899, 1999, doi: 10.1016/S1388-2457(99)00238-2.

[54] and S. K. Josef Parvizi, "Human Intracranial EEG: Promises and Limitations," Physiol Behav, vol. 176, no. 5, pp. 139–148, 2017, doi: 10.1038/s41593-018-0108-2.Human.

[55] W. Surbeck et al., "The combination of subdural and depth electrodes for intracranial EEG investigation of suspected insular (perisylvian) epilepsy," Epilepsia, vol. 52, no. 3, pp. 458–466, 2011, doi: 10.1111/j.1528-1167.2010.02910.x.

[56] S. P. Singh, "Magnetoencephalography: Basic principles," Ann Indian Acad Neurol, vol. 17, no. SUPPL. 1, 2014, doi: 10.4103/0972-2327.128676.

[57] G. H. Glover, "Overview of functional magnetic resonance imaging," Neurosurgery Clinics of North America, vol. 22, no. 2, pp. 133–139, 2011, doi: 10.1016/j.nec.2010.11.001.

[58] "Bergen fMRI Group | University of Bergen." https://www.uib.no/en/rg/fmri (accessed Jun. 05, 2022).

[59] P. W. K. William O. Tatum, Aatif M. Husain, Selim R. Benbadis, Handbook of EEG interpretation. 2014.

[60] L. H. Koopmans, "Digital Filters," The Spectral Analysis of Time Series, pp. 165–209, 1995, doi: 10.1016/B978-012419251-5/50008-9.

[61] C. J. Chu et al., "Emergence of stable functional networks in long-term human electroencephalography," Journal of Neuroscience, vol. 32, no. 8, pp. 2703–2713, 2012, doi: 10.1523/JNEUROSCI.5669-11.2012.

[62] A. Adebimpe, A. Aarabi, E. Bourel-Ponchel, M. Mahmoudzadeh, and F. Wallois, "EEG resting state functional connectivity analysis in children with benign epilepsy with centrotemporal spikes," Frontiers in Neuroscience, vol. 10, no. MAR, pp. 1–9, 2016, doi: 10.3389/fnins.2016.00143.

[63] P. Goetz et al., "Scalp EEG markers of normal infant development using visual and computational approaches," Proceedings of the Annual International Conference of the IEEE Engineering in Medicine and Biology Society, EMBS, pp. 6528–6532, 2021, doi: 10.1109/EMBC46164.2021.9629909.

[64] P. J. Durka, H. Klekowicz, K. J. Blinowska, and W. Szelenberger, "A Simple System for Detection of EEG Artifacts in Polysomnographic Recordings," vol. 50, no. 4, pp. 2001–2003, 2003.

[65] D. v. Moretti et al., "Computerized processing of EEG-EOG-EMG artifacts for multi-centric studies in EEG oscillations and event-related potentials," International Journal of Psychophysiology, vol. 47, no. 3, pp. 199–216, 2003, doi: 10.1016/S0167-8760(02)00153-8.

[66] M. A. Kramer, U. T. Eden, S. S. Cash, and E. D. Kolaczyk, "Network inference with confidence from multivariate time series," Physical Review E - Statistical, Nonlinear, and Soft Matter Physics, vol. 79, no. 6, pp. 1–13, 2009, doi: 10.1103/PhysRevE.79.061916.

[67] C. J. Stam, G. Nolte, and A. Daffertshofer, "Phase lag index: Assessment of functional connectivity from multi channel EEG and MEG with diminished bias from common sources," Human Brain Mapping, vol. 28, no. 11, pp. 1178–1193, 2007, doi: 10.1002/hbm.20346.

[68] D. K. Hu, L. Y. Li, B. A. Lopour, and E. A. Martin, "Schizotypy dimensions are associated with altered resting state alpha connectivity," International Journal of Psychophysiology, vol. 155, no. May, pp. 175–183, 2020, doi: 10.1016/j.ijpsycho.2020.06.012.

[69] J. Debenham and R. R. Wagner, Lecture Notes in Computer Science: Preface, vol. 3588. 2005.

[70] "MATLAB - MathWorks - MATLAB & Simulink." https://www.mathworks.com/products/matlab.html (accessed Jun. 05, 2022).

[71] D. Kuhlman, "A Python Book," A Python Book, pp. 1–227, 2013.

[72] E. st. Louis et al., Electroencephalography (EEG): An Introductory Text and Atlas of Normal and Abnormal Findings in Adults, Children, and Infants. 2016. doi: 10.5698/978-0-9979756-0-4.

[73] "Precision 5820 High Performance Tower Desktop Workstation | Dell USA." https://www.dell.com/en-us/work/shop/workstations-isv-certified/precision-5820-tower-workstation/spd/precision-5820-workstation/xctopt5820us_4 (accessed Jun. 05, 2022).

[74] "Dell 24 FHD Monitor: S2421HSX | Dell USA." https://www.dell.com/en-us/work/shop/dell-24-monitor-s2421hsx/apd/210-axim/monitors-monitor-accessories?gacd=9646510-1025-5761040-266794296-0&dgc=st&ds_rl=1282786&gclid=Cj0KCQjw4uaUBhC8ARIsANUuDjUhMArKO8vUDMxu60Vpk80Ql36D5b-dzmPuc9aJKyFlF7MTPXmiRHkaAnEPEALw_wcB&gclsrc=aw.ds&nclid=7ZQJQrGSm9qXWavktYte6mUnuLJW8TRoSOJLCmg1ibdvjF-JUEqCTLSrcKC_rjTxWnf_QuPFE8WOd3AVhFlmV1-WgqAgynimnd2RA61Oo2yJDVRyLfsHIONEmtyhG5KY (accessed Jun. 05, 2022).

[75] "Dell Pro Wireless Keyboard and Mouse – KM5221W | Dell USA." https://www.dell.com/en-us/work/shop/dell-pro-wireless-keyboard-and-mouse-km5221w/apd/580-ajis/pc-accessories (accessed Jun. 05, 2022).

[76] "Pricing and Licensing - MATLAB & Simulink." https://es.mathworks.com/pricing-licensing.html (accessed Jun. 05, 2022).

9. APPENDIX

Appendix 1: State of the Art - Papers

Paper	Authors	Data	Aim of study
Hypsarrhythmia assessment exhibits poor interrater reliability: A threat to clinical trial validity	Hussain et al.	EEG	Diagnosis
A study of spike density on EEG in West syndrome	Oka et al.	EEG	Diagnosis
Paroxysmal fast activity: an interictal scalp EEG marker of epileptogenesis in children	Wu et al.	EEG	Diagnosis
Improving the inter-rater agreement of hypsarrhythmia using a simplified EEG grading scale for children with infantile spasms	Mytinger et al.	EEG	Diagnosis
A reliable interictal EEG grading scale for children with infantile spasms - The 2021 BASED score	Mytinger et al.	EEG	Diagnosis Treatment outcome
Predictive value of EEG findings at control of epileptic spasms for seizure relapse in patients with West Syndrome	Yamada et al.	EEG	Treatment outcome
Prediction of infantile spasms recurrence after ACTH Therapy	Millichap et al.	EEG	Long-term outcome prediction and relapse
The prognostic value of sleep spindles in long-term outcome of West Syndrome	Spenner et al.	EEG	Long-term outcome prediction and relapse
Assessing risk of relapse among children with infantile spasms using the Based Score after ACTH treatment: a retrospective study	Wan et al.	EEG	Long-term outcome prediction and relapse

Table 1: Infantile Spasms (IS) visual inspection techniques for diagnosis, treatment outcome and long-term outcome prediction and relapse.

Paper	Authors	Data	Technique/s	Aim
Effect of interictal epileptiform discharges on EEG-based functional connectivity networks.	Hu et al.	EEG	Functional connectivity (cross-correlation)	Diagnosis
Quantitative characteristics of hypsarrhythmia in Infantile Spasms	Smith et al.	EEG	Amplitude, Spectral Power	Diagnosis
Computational characteristics of interictal EEG as objective markers of epileptic spasms	Smith et al.	EEG	Amplitude, Spectral Power, Entropy, long-range temporal correlations (DFA), Functional connectivity (cross-correlation, PLI)	Diagnosis
Brain connectivity in West Syndrome	Burroughs et al.	EEG	Functional connectivity (coherence), Spectral Power	Diagnosis
Electroencephalography based functional networks in newly diagnosed childhood epilepsies	Diessen et al.	EEG	Spectral Power, Functional connectivity (PLI), Minimum spanning tree (MST).	Diagnosis
Neuronal networks in West Syndrome as revealed by source analysis and renormalized partial directed coherence	Japaridze et al.	EEG	Coherence (DICS), Directionality analysis (RPDC)	Diagnosis
Automated preprocessing and phase-amplitude coupling analysis of scalp EEG discriminates infantile spasms from controls during wakefulness	Miyakoshi et al.	EEG	Dellta-gamma modulation index (MI)	Diagnosis
Scalp EEG interictal high frequency oscillations as an objective biomarker of infantile spasms	Nariai et al.	EEG	HFOs, SWA	Diagnosis
Emerging roles of network analysis for epilepsy	Stacey et al.	EEG, iEEG, DWI	Functional connectivity	Diagnosis
Complex observation of scalp fast (40-150 Hz) oscillations in West syndrome and related disorders with structural brain pathology.	Kobayashi et al.	EEG	FOs/TF analysis	Diagnosis
Fast oscillation dynamics during hypsarrhythmia as a localization biomarker	Kim et al.	EEG	FOs/ERSP	Diagnosis
Ictal high-frequency oscillations on scalp EEG recordings in symptomatic West syndrome	Iwatani et al.	EEG	HFOs	Diagnosis
Longitudinal correspondence of epilepsy and scalp EEG fast (40-200 Hz) oscillations in pediatric patients with tuberous sclerosis complex	Tsuchiya et al.	EEG	FOs (burden)	Diagnosis
Increased electroencephalography connectivity precedes epileptic spasm onset in infants with tuberous sclerosis complex	Davis et al.	EEG	Functional connectivity (FC): Mutual information (MI)	Diagnosis

Developing a novel epileptic discharge localization algorithm for electroencephalogram infantile spasms during hypsarrhythmia	Traitruengsakul et al.	EEG	TF	Diagnosis
Epileptogenic modulation index and synchronization in hypsarrhythmia of West syndrome secondary to perinatal arterial ischemic stroke	Suzuki et al.	EEG	Modulation index (MI) & Synchronization likelyhood (SL)	Diagnosis
Hypsarrhythmia in epileptic spasms: Synchrony in chaos	Nenadovic et al.	EEG	Mean phase coherence	Diagnosis
Automated detection of ripple oscillations in long-term scalp EEG from patients with infantile spasms	McCrimmon et al.	EEG	HFOs	Diagnosis Treatment outcome
A storm of fast (40-150 Hz) oscillations hypsarrhythmia in West syndrome	Kobayashi et al.	EEG	FOs/TF analysis	Diagnosis Treatment outcome
Automatic detection of interictal ripples on scalp EEG to evaluate the effect and prognosis of ACTH therapy in patients whith infantile spasms	Wang et al.	EEG	HFOs	Diagnosis Treatment outcome
Epileptogenic modulation index and synchronization in hypsarrhythmia of West syndrome secondary to perinatal arterial ischemic stroke	Tanritanir et al.	EEG	Delta power and Delta Coherence	Treatment prediction Treatment outcome
Electroencephalography complexity in infantile spasms and its association with treatment response	Chu et al.	EEG	Multiscale entropy (MSE)	Treatment prediction

Table 2: Infantile Spasms (IS) computational analysis techniques for diagnosis, treatment outcome, treatment prediction, and long-term outcome prediction and relapse.

Appendix 2: Pre-processing outline code

```
[info, EEG_raw] = edfreadUntilDone("L010.EEG7.edf"); % Loading edf file (data)

EEG_data = EEG_raw(1:19,:); % Selection of 19 electrodes

% Removing zeros from the end of the data
diff_EEG = diff(EEG_data,1,2);
diffIsZero = diff_EEG == 0;
impChecks = double(diffIsZero);
sumImpCheck = sum(impChecks);
impCheckVec = sumImpCheck==19;
impCheckArts = find(impCheckVec==1);
diff_impCheckArts = diff(impCheckArts);
if sum(diff_impCheckArts) == size(diff_impCheckArts,2)
    EEG_data(:,impCheckArts(1):impCheckArts(size(impCheckArts,2)))=[];
end

% Automatic Artifact Detection
[autoArts] = artifact_detector_RJS_041119(EEG_data,200,7.5,0.9,1);

% Filtering
[EEG_filt,time,fs,labels,CAR_filt, allArtIndex, artifacts] = tfg_cleanData (EEG_data,
info,'broadband','CAR',autoArts);
artifacts_ind = artifacts * fs;

% Connectivity calculation
[all_connectMat, select_z_binary, connectMat,z_binary,z,nWin,criticalZ,lagAtMaxCC,lagAtZero,EEG_window,EEG_clean]
= tfg_calculate_ConnectVal(EEG_filt,fs,CAR_filt, artifacts_ind, min_len);
```

Appendix 3: Filtering function

```
function [EEG_filt,time,fs,labels,CAR_filt, allArtIndex, artifacts] = tfg_cleanData
(eeg_record,info,pickAFilter,reReference,autoArts)

labels = info.label;
labels(20:size(labels,2)) = [];

fs = 200;
time = (1:size(eeg_record,2))/fs;

artifacts = [autoArts.times]; %start and end times

% Check that all artifacts go from an earlier time to a later time
for a=1:size(artifacts,1)
   if artifacts(a,2)<artifacts(a,1)
        temp = artifacts(a,2);
        artifacts(a,2) = artifacts(a,1);
        artifacts(a,1)=temp;
    end
end

% Re-reference to the specified montage
EEG = eeg_record;
if ~isempty(reReference)
    switch reReference
        case 'CAR'
            CAR = mean(EEG(1:19,:),1);
            EEG_reref = EEG-repmat(CAR,size(EEG,1),1);
            EEG_reref = EEG_reref(1:19,:);
        case 'EAR'
            ear = (EEG(20,:)+EEG(21,:))./2;
            EEG_reref = EEG-repmat(ear,size(EEG,1),1);
            EEG_reref = EEG_reref(1:19,:);
    end
else
    EEG_reref = EEG;
    EEG_reref = EEG_reref(1:19,:);
end

%Filtering of the data
if ischar(pickAFilter)
switch pickAFilter
    case 'delta'
        [filter] = pickFilter(pickAFilter,fs);
```

```
        EEG_filt = filtfilt(filter,1,EEG_reref');
        EEG_filt = EEG_filt';
        if strcmp(reReference,'CAR')==1
            CAR_filt = filtfilt(filter,1,CAR');
            CAR_filt = CAR_filt';
        end
    case 'theta'
        [filter] = pickFilter(pickAFilter,fs);
        EEG_filt = filtfilt(filter,1,EEG_reref');
        EEG_filt = EEG_filt';
        if strcmp(reReference,'CAR')==1
            CAR_filt = filtfilt(filter,1,CAR');
            CAR_filt = CAR_filt';
        end
    case 'alpha'
        [filter] = pickFilter(pickAFilter,fs);
        EEG_filt = filtfilt(filter,1,EEG_reref');
        EEG_filt = EEG_filt';
        if strcmp(reReference,'CAR')==1
            CAR_filt = filtfilt(filter,1,CAR');
            CAR_filt = CAR_filt';
        end
    case 'beta'
        [filter] = pickFilter(pickAFilter,fs);
        EEG_filt = filtfilt(filter,1,EEG_reref');
        EEG_filt = EEG_filt';
        if strcmp(reReference,'CAR')==1
            CAR_filt = filtfilt(filter,1,CAR');
            CAR_filt = CAR_filt';
        end
    case 'broadband'
        [filter] = pickFilter(pickAFilter,fs);
        EEG_filt = filtfilt(filter,1,EEG_reref');
        EEG_filt = EEG_filt';
        if strcmp(reReference,'CAR')==1
            CAR_filt = filtfilt(filter,1,CAR');
            CAR_filt = CAR_filt';
        end
    case 'muscle'
        [filter] = pickFilter(pickAFilter,fs);
        EEG_filt = filtfilt(filter,1,EEG_reref');
        EEG_filt = EEG_filt';
        if strcmp(reReference,'CAR')==1
            CAR_filt = filtfilt(filter,1,CAR');
            CAR_filt = CAR_filt';
        end
    case 'none'
        EEG_filt = EEG_reref;
%         CAR_filt = CAR;
end
else
    filter = pickAFilter;
    EEG_filt = filtfilt(filter,1,EEG_reref');
    EEG_filt = EEG_filt';
    if strcmp(reReference,'CAR')==1
        CAR_filt = filtfilt(filter,1,CAR');
        CAR_filt = CAR_filt';
    end
end

% Get vector indices corresponding to all artifacts
if isempty(artifacts)
    allArtIndex=[];
else
    allArtIndex=[];
    art = round(artifacts*fs);  % convert times to indices
    for i=1:size(artifacts,1)
        allArtIndex=[allArtIndex,art(i,1):art(i,2)];
    end
end

allArtIndex = sort(allArtIndex);
allArtEAR = allArtIndex(2:end);

%%Plot of the signal
time_all = (1:size(eeg_record,2))/fs; %total time, needed for plotting
color =['y', 'm','c','r','g','b','k'];
% Plot raw data
figure;
```

```
counter=1;
for i=1:size(eeg_record,1)
    shift=(i-1)*800;
    yax=eeg_record(i,:)+shift;
    plot(time_all,yax,color(counter))
    hold on;
    counter=counter+1;
    if counter>size(color,2)
        counter=1;
    end
end
%hleg1=legend('1. FP1','2. FP2','3. F3','4. F4','5. C3','6. C4','7. P3','8. P4','9. 01','10. 02','11. F7','12.F8',
'13.T3', '14.T4', '15.T5', '16.T6', '17.Fz', '18.Cz', '19.Pz');
%set(hleg1,'Location','EastOutside');
title('L001.EEG1 - EEG - raw data','FontSize', 18);
xlabel("Time(sec)");
yticks([0 800 1600 2400 3200 4000 4800 5600 6400 7200 8000 8800 9600 10400 11200 12000 12800 13600 14400])
yticklabels({'FP1', 'FP2', 'F3', 'F4', 'C3', 'C4', 'P3', 'P4', 'O1', 'O2', 'F7', 'F8', 'T3', 'T4', 'T5', 'T6',
'Fz', 'Cz', 'Pz'})
ylabel("Amplitude (mV)");

% Plot EEG data after removing electrodes and (artifacts) & rereferencing
figure; hold on;
counter=1;
for i=1:size(EEG_filt,1)
    shift=(i-1)*800;
    plot(time,EEG_filt(i,:)+shift,color(counter))
    %plot(time,EEG_filt(i,:)+shift,'k')
    counter=counter+1;
    if counter>size(color,2)
        counter=1;
    end
end
%hleg1=legend('1. FP1','2. FP2','3. F3','4. F4','5. C3','6. C4','7. P3','8. P4','9. 01','10. 02','11. F7','12.F8',
'13.T3', '14.T4', '15.T5', '16.T6', '17.Fz', '18.Cz', '19.Pz');
%set(hleg1,'Location','EastOutside');
title('L001.EEG1 - EEG - filtered and re-ref', 'FontSize', 18);
xlabel("Time(sec)");
yticks([0 800 1600 2400 3200 4000 4800 5600 6400 7200 8000 8800 9600 10400 11200 12000 12800 13600 14400])
yticklabels({'FP1', 'FP2', 'F3', 'F4', 'C3', 'C4', 'P3', 'P4', 'O1', 'O2', 'F7', 'F8', 'T3', 'T4', 'T5', 'T6',
'Fz', 'Cz', 'Pz'})
ylabel("Amplitude (mV)");

clear eeg_info eeg_record
return
end
```

Appendix 4: Automated Artifact Detection

```
function [autoArts] = artifact_detector_RJS_041119(eeg_record,fs,stdAbove,buffer,channelsInvolved)

% filter data the same way they do to clinically view

% Create filters - these were compared to Nihon Kohden viewer in Aug 2015
tau = 0.1;  % time constant in Nihon Kohden
cutoff = 1/(2*pi*tau); % cutoff frequency is a function of time constant
[b,a] = butter(1, cutoff/(fs/2), 'high');
[b2,a2] = butter(3, 40/(fs/2), 'low');

% Filter the data - Nihon Kohden does not use zero-phase filters
eeg_filt = filter(b,a,eeg_record',[],1);
eeg_filt = -filter(b2,a2,eeg_filt,[],1); % POSITIVE DOWN
eeg_filt = eeg_filt';

meanEEG = mean(eeg_filt,2);
stdEEG = std(eeg_filt,0,2);

% set an absolute threshold that an artifact must be over 200 uV.
stdEEG(stdEEG<(200/stdAbove)) = 200/stdAbove;

possArts = zeros(size(eeg_filt));
for j=1:size(eeg_filt,1)
    possArts(j,:) = abs(eeg_filt(j,:)-meanEEG(j))>stdAbove*stdEEG(j);
end

% get logical vector for any artifacts
sumArtsVec = sum(possArts,1);
artsVec = sumArtsVec>channelsInvolved-1;
```

```
% pad around the artifact to ensure you get the entire event (buffer = # of seconds)
indicesArts = find(artsVec);
for k=1:size(indicesArts,2)
    if indicesArts(k)-buffer*fs<=0
        artsVec(1:indicesArts(k)+buffer*fs) = 1;
    elseif indicesArts(k)+buffer*fs>=size(eeg_record,2)
        artsVec(indicesArts(k)-buffer*fs:end) = 1;
    else
        artsVec(indicesArts(k)-buffer*fs:indicesArts(k)+buffer*fs) = 1;
    end
end

% get it into times that can be read into the artifact_marking code
% difference between indices vector will show which have a difference more
% than 1
fullIndArts = find(artsVec);
diffVec = diff(fullIndArts);
largeDiff = find(diffVec~=1); %find when the artifact sample is non-consecutive
artTimes = [];
if ~isempty(fullIndArts)
    artTimes = zeros(1,2);
    artTimes(1,1) = fullIndArts(1)./fs;
    for m = 1:size(largeDiff,2)
        artTimes(m,2) = fullIndArts(largeDiff(m))./fs;
        artTimes(m+1,1) = fullIndArts(largeDiff(m)+1)./fs;
    end
    artTimes(size(largeDiff,2)+1,2) = fullIndArts(end)./fs;
end

% add artifacts from impedance checks

diff_EEGrec = diff(eeg_record,1,2);
diffIsZero = diff_EEGrec == 0;
impChecks = double(diffIsZero);
sumImpCheck = sum(impChecks);
impCheckVec = sumImpCheck>8;

impCheckArts = find(impCheckVec==1);

newArts = [];
if ~isempty(impCheckArts)
    diffVec2 = diff(impCheckArts);
    largeDiff2 = find(diffVec2~=1); %find when the artifact sample is non-consecutive

    newArts = zeros(1,2);
    newArts(1,1) = impCheckArts(1)./fs;
    for p = 1:size(largeDiff2,2)
     newArts(p,2) = impCheckArts(largeDiff2(p))./fs;
     newArts(p+1,1) = impCheckArts(largeDiff2(p)+1)./fs;
    end
    newArts(size(largeDiff2,2)+1,2) = impCheckArts(end)./fs;
end
artTimes = [artTimes; newArts];

autoArts.times = artTimes;
autoArts.general = ones(1,size(artTimes,1));
autoArts.eye = zeros(1,size(artTimes,1));
autoArts.ear = zeros(1,size(artTimes,1));

end
```

Appendix 5: Connectivity calculation

```
function [all_connectMat, select_z_binary, connectMat,z_binary,z,nWin,criticalZ,lagAtMaxCC,lagAtZero, EEG_window,
EEG_clean] = tfg_calculate_ConnectVal(EEG_filt,fs,CAR_filt,artifacts, min_len)

% ========================= CROSS CORRELATION ========================
% Calculate cross correlation for all 1-second windows
maxLag=0.2*fs;  % max lags (in indices)
nElec=size(EEG_filt,1); % number of remaining electrodes after preprocessing
nTime=size(EEG_filt,2); % number of time points after preprocessing
nWin = fix(nTime/fs);

lagAtMaxCC=zeros(nElec,nElec,nWin);
z=zeros(nElec,nElec,nWin);
partialRemove = zeros(nElec,nElec,nWin);
```

```
% Loop over all 1-second windows, run crossCorrFn
EEG_clean = []; %vector for EEG clean data, no artifacts
for i=1:(nTime/fs)
    tEnd=i*fs;
    tStart=tEnd-fs+1;
    artif_affected = 0;
    for j=1:size(artifacts,1)
        artif_start = artifacts(j,1);
        artif_end = artifacts(j,2);
        if ((artif_start < tEnd) && (tEnd < artif_end)) || ...
                ((tStart < artif_start) && (artif_end < tEnd)) || ...
                ((artif_start < tStart) && (tStart < artif_end)) || ...
                ((artif_start < tStart) && (tEnd < artif_end))
            artif_affected = 1;
            break
        end
    end
    %fprintf("tStart: %i / tEnd: %i / artif: %i\n", tStart, tEnd, artif_affected);
    if artif_affected == 1
        continue
    end
    EEG_window=EEG_filt(:,tStart:tEnd);
    CAR_window=CAR_filt(tStart:tEnd);
    [zInWindow,lagInWindow,partial]=crossCorrFn(fs, maxLag, EEG_window, EEG_window,1, CAR_window);
    EEG_clean=[EEG_clean EEG_window]; %EEG data with no artifacts

    lagAtMaxCC(:,:,i)=lagInWindow;
    z(:,:,i)=zInWindow;
    partialRemove(:,:,i) = partial;
end

% ==================== PERMUTATION RESAMPLING ==========================
% Shift the data in time and find the maximum cross correlation that can
% occur by chance
nIter=1000;
threshold=0.95*nIter;  % percentile for critical z-value; needs to be an integer
CAR_window=zeros(1,size(CAR_window,2));
z_shift = zeros(nElec,nElec,nIter);

for i=1:nIter
    shift=randperm(size(EEG_clean,2)-fs,2);%two random values (min separation 1 sec)

    EEG_shifted=circshift(EEG_clean',shift(1))'; % shift filtered data
    elec1=EEG_clean(:,shift(2):(shift(2)+fs)); % signal 1 - original
    elec2=EEG_shifted(:,shift(2):(shift(2)+fs)); % signal 2 - shifted

    %cross correlation for the random 1s interval
    [z_shift(:,:,i),~,~]=crossCorrFn(fs, maxLag, elec1, elec2,0, CAR_window);
end

% Sort max cross correlation values and determine critical z value
criticalZ = zeros(nElec);
for i=1:nElec
    for j=(i+1):nElec
        allIter = sort(squeeze(z_shift(i,j,:)));
        criticalZ(i,j) = allIter(threshold);
    end
end

% Compare calculated z-value to threshold based on permutation resampling
% Each window of data gets a binary value (1 if significant)
z_binary=zeros(nElec,nElec,nWin);
lagAtZero=zeros(nElec,nElec,nWin);
for win=1:nWin % for each window
    for j=1:nElec
        for k=(j+1):nElec  % skip self-comparisons (j=k)
            %if maximum occurs at 0 lag
            if lagAtMaxCC(j,k,win)==0
                lagAtZero(j,k,win)=1; % z_binary is also zero (already set to zero)
                lagAtZero(k,j,win)=1;
            else
                % Compare to critical value, 1 = significant
                z_binary(j,k,win) = (z(j,k,win)>=criticalZ(j,k));
                z_binary(k,j,win) = (z(j,k,win)>=criticalZ(j,k));
            end
        end
    end
end
```

```
all_connectMat = zeros(19,19,(min_len/fs));
for m=1:1000
    rng(13) %to get consistent results
   % Desired number of window indices from 1 to size of data with repetition
    nWin_rnd = randi(size(z_binary,3), 1, min_len/fs);
    select_z_binary = z_binary(:,:,nWin_rnd);
    all_connectMat(:,:,m) = mean(select_z_binary,3);
end

connectMat = mean(all_connectMat,3);
% connectMat = mean(z_binary,3);
% connectVal = sum(sum(connectMat));

end
```

Appendix 6: Representation of cross-correlation matrix

```
lim = [0,0.4]; %value limits

figure()
imagesc(s1eeg1)
colormap jet;
colorbar();
caxis(lim);
title("Cross-correlation matrix (L001.EEG1 - thresh)", "FontSize", 17);
xticks(1:19);
xticklabels(labels)
yticks(1:19);
yticklabels(labels)
```

Appendix 7: Connectivity topographic plot

```
% Setup
c = jet(100);
% Percentile thresholding
triang = triu(connectMat,1);
nonzero_triang = nonzeros(triang);
sort_vals = sort(nonzero_triang);
sig = prctile(sort_vals,90,'all');
multiplier = 250; %this number increases the connectivity value so it matches the color scale

load("chanlocs_CHOC.mat");
chanloc2 = chanloc;
chanloc2_labels = cell(1,19);

sigSum2 = zeros(19);
sigSum1 = zeros(19);

X = zeros(1,19);
Y = zeros(1,19);
Z = zeros(1,19);

% Extracting chanloc locations
for i=1:19
    chanloc2_labels{i} = chanloc2(i).labels;
    X(i) = chanloc2(i).X;
    Y(i) = chanloc2(i).Y;
    Z(i) = chanloc2(i).Z;
end
X = X/200 + 0.5;
Y = Y/200 + 0.5;
Z = Z/200 + 0.5;

nChan = 19; % 19 electrodes
sigZ = connectMat; %adjacency matrix
percentSig(:,:) = sigZ(1:19,1:19);

% Plot black dot at each electrode
for i=1:19
    figure(2)
    ylim([-0.1 1.1])
    xlim([-0.1 1.1])
    title("Connectivity plot (L006.EEG3)")

    % Electrode names
    text(X(i), Y(i)-0.015, chanloc2_labels{i});
```

```
    camroll(-90)
    hold on
    plot(X(i),Y(i),'k.')
    th = linspace(0, 2*pi, 100);
    R = 0.5;  %or whatever radius you want
    xh = R*cos(th)+0.5;
    yh = R*sin(th)+0.5;


    % For top ear
    th = linspace(0, pi, 100);
    R = 0.05;  %or whatever radius you want
    xte = R*cos(th) + X(14);
    yte = R*sin(th) + 1;

    % For bottom ear
    th = linspace(0, -pi, 100);
    R = 0.05;  %or whatever radius you want
    xbe = R*cos(th) + X(6);
    ybe = R*sin(th) + 0;

    % Plot head, ears
    plot(xh,yh,'k'); %axis equal;
    plot(xte,yte,'k');
    plot(xbe,ybe,'k');
    % Plot nose
    plot([1 1.05], [Y(4)-0.065 mean(Y([4,12]))], 'k')
    plot([1 1.05], [Y(12)+0.065 mean(Y([4,12]))], 'k')
end

close all

% Actually plotting the network
for i=1:19

    % Plotting our electrode locations
    hold on
    plot(X(i),Y(i),'k*')
    colormap jet
    ylim([-0.1 1.1])
    xlim([-0.1 1.1])
    title('L005.EEG5')


    camroll(-90) % rotate our head to right orientation

    % Colorbar BASED ON OUR MULTIPLIER
    blah3 = colorbar;
    title(blah3, '')
    caxis([0 0.4]) % color axis maximum

    % Electrode names
    text(X(i), Y(i)-0.015, labels{i});

    % Face
    plot(xh,yh,'k'); %axis equal;

    % Ears
    plot(xte,yte,'k');
    plot(xbe,ybe,'k');

    % Plot nose
    plot([1 1.05], [Y(1)-0.065 mean(Y([1,2]))], 'k')
    plot([1 1.05], [Y(2)+0.065 mean(Y([1,2]))], 'k')

    for j=(i+1):19

        if percentSig(i,j)>=sig
            xvec = [X(j) X(i)];
            yvec = [Y(j) Y(i)];

            colorIndex = floor(percentSig(i,j)*multiplier);

            % Functional connectivity map
            plot(xvec, yvec, 'color', c(colorIndex,:),'linewidth',2)
        end
    end
end
```

Appendix 8: Number of connections above threshold

```
% Calculations for 1 patient, different thresholds
connections = ["s1eeg1", "s1eeg2", "s1eeg3", "s1eeg4", "s1eeg5"];
thres = [0.1, 0.15, 0.2, 0.25];
val = zeros(length(thres), length(connections));
for i=1:length(thres)
    limit = thres(i);

    for j=1:length(connections)
        matrix = eval(connections(j));
        val(i,j) = nnz(matrix>limit)/2;
    end
end

x = 1 : length(connections);
plot(x,val(1,:), '-or', 'MarkerFaceColor', 'r');
hold on
plot(x, val(2,:), '-ok', 'MarkerFaceColor', 'k');
hold on
plot(x, val(3,:), '-ob', 'MarkerFaceColor', 'b');
hold on
plot(x, val(4,:), '-og', 'MarkerFaceColor', 'g');
hold off
xticks(x)
xticklabels({'EEG 1','EEG 2','EEG 3','EEG 4', 'EEG 5'})
ylabel('Sum of strong connections')
title('Subject 01: Strong Connections')
legend("> 0.10", "> 0.15", "> 0.20", "> 0.25")
```

Appendix 9: Mean strength of connections above percentile

```
%Calculation for 1 subjects and different percentiles
percentile = [95, 90, 85, 80];
mean_mat = zeros(length(percentile), length(connections1));

for i=1:length(percentile)
    percent_val = percentile(i);
    for j=1:length(connections1)
        matrix = eval(connections1(j));

        % Find percentile threshold
        triang = triu(matrix,1);
        nonzero_triang = nonzeros(triang);
        sort_vals = sort(nonzero_triang);
        threshold = prctile(sort_vals, percent_val, 'all');

        % Calculate mean of values above threshold
        tf = matrix > threshold;
        mean_mat(i,j) = mean(reshape(matrix(tf),1,[]));
    end

end

x = 1 : length(connections1);

plot(x,mean_mat(1,:), '-or', 'MarkerFaceColor', 'r');
hold on
plot(x, mean_mat(2,:), '-ok', 'MarkerFaceColor', 'k');
hold on
plot(x, mean_mat(3,:), '-ob', 'MarkerFaceColor', 'b');
hold on
plot(x, mean_mat(4,:), '-og', 'MarkerFaceColor', 'g');
hold off
xticks(x)
%xticklabels({'IS diagnosis','','', 'LGS diagnosis', ''})
xticklabels({'EEG 1','EEG 2','EEG 3','EEG 4', 'EEG 5'})
ylabel('Mean strength above percentile')
title('Subject 01: Mean strength')
legend("95th percentile", "90th percentile", "85th percentile", "80th percentile")
```